Secondary Production of Gaseous Nitrated Phenols in Polluted Urban Environments

Cheng, Xi

2021-04-20

Cheng , X , Chen , Q , Li , Y , Huang , G , Liu , Y , Lu , S , Zheng , Y , Qiu , W , Lu , K , Qiu , X , Bianchi , F , Yan , C , Yuan , B , Shao , M , Wang , Z , Canagaratna , M R , Zhu , T , Wu , Y & Zeng , L 2021 , ' Secondary Production of Gaseous Nitrated Phenols in Polluted Urban Environments ' , Environmental Science & Technology , vol. 55 , no. 8 , pp. 4410-4419 . https://doi.org/10.1021/acs.e

http://hdl.handle.net/10138/353878
https://doi.org/10.1021/acs.est.0c07988

unspecified
acceptedVersion

Secondary Production of Gaseous Nitrated Phenols in Polluted Urban Environments

Xi Cheng,[1] Qi Chen,[1,] Yongjie Li,[2] Guancong Huang,[1] Ying Liu,[1] Sihua Lu,[1] Yan Zheng,[1] Wanyi Qiu,[1] Keding Lu,[1] Xinghua Qiu,[1] Federico Bianchi,[3] Chao Yan,[3,4] Bin Yuan,[5] Min Shao,[1,5] Zhe Wang,[6] Manjula R. Canagaratna,[7] Tong Zhu,[1] Yusheng Wu,[1] Limin Zeng[1]*

[1]State Key Joint Laboratory of Environmental Simulation and Pollution Control, BIC-ESAT and IJRC, College of Environmental Sciences and Engineering, Peking University, Beijing, China

[2]Department of Civil and Environmental Engineering, Faculty of Science and Technology, University of Macau, Taipa, Macau, China

[3]Institute for Atmospheric and Earth System Research, Faculty of Science, University of Helsinki, Helsinki, Finland

[4]Aerosol and Haze Laboratory, Beijing Advanced Innovation Center for Soft Matter Science and Engineering, Beijing University of Chemical Technology, Beijing, China

[5]Institute for Environmental and Climate Research, Jinan University, Guangzhou, China

[6]Division of Environment and Sustainability, The Hong Kong University of Science and Technology, Hong Kong, China

[7]Aerodyne Research Inc., Billerica, MA, USA

***Correspondence to:**

Qi Chen (Email: qichenpku@pku.edu.cn)

TOC ART

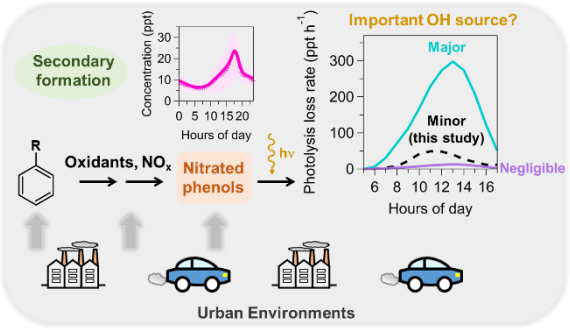
Secondary formation
Concentration (ppt)
30
20
10
0
0 5 10 15 20
Hours of day
R
Oxidants, NOx
Nitrated phenols
hv
Photolysis loss rate (ppt h-1)
Important OH source?
Major
Minor (this study)
Negligible
300
200
100
0
6 8 10 12 14 16
Hours of day
Urban Environments

ABSTRACT

Nitrated phenols (NPs) are important atmospheric pollutants that affect air quality, radiation, and health. Recent development of time-of-flight chemical ionization mass spectrometer (ToF-CIMS) allows quantitative online measurements of NPs for a better understanding of their sources and environmental impacts. Herein, we deployed nitrate ions as reagent ions in the ToF-CIMS and quantified six classes of gaseous NPs in Beijing. The concentrations of NPs are in the range of 1 to 520 ng m^{-3}. Nitrophenol (NPh) has the greatest mean concentration. Dinitrophenol (DNP) shows the greatest haze-to-clean concentration ratio, which may be associated with aqueous production. The high concentrations and distinct diurnal profiles of NPs indicate strong secondary formation to overweigh losses, driven by high emissions of precursors, strong oxidative capacity, and high NO_x levels. The budget analysis on the basis of our measurements and box-model calculations suggest a minor role of the photolysis of NPs (< 1 ppb h^{-1}) in producing OH radicals. NPs therefore cannot explain the underestimated OH production in urban environments. Discrepancies between these results and the laboratory measurements of NP photolysis rates indicate the need for further studies aimed at understanding the production and losses of NPs in polluted urban environments.

INTRODUCTION

Nitrated phenols (NPs) that have one or more hydroxyl (-OH) and nitro (-NO_2) groups on the aromatic ring are important atmospheric pollutants. They may partition between gas and condense phases and hence widely exist in air, clouds, rain water, fog, and snow.[1] The photolysis of gaseous NPs may produce nitrous acid (HONO) and hydroxyl radicals (OH), affecting the atmospheric oxidation capacity and the distribution of NO_x.[2-5] The particle-phase NPs are major particulate chromophores that affect the radiation balance.[6,7]

Vehicles, coal burning, biomass burning, and industry are common primary sources of NPs. Secondary NPs may be formed by the gas- or condensed-phase nitration of phenols or the reaction of NO_2 with phenoxy radicals produced by other aromatic precursors (e.g., benzaldehyde).[1] Atmospheric concentrations of NPs have been measured mostly by off-line methods using high performance liquid chromatography (HPLC) or gas chromatography-mass spectrometry (GC-MS). In recent years, time-of-flight chemical ionization mass spectrometers (ToF-CIMS) have been used to quantify the NPs in both the gas- and particle-phase with a time resolution of seconds to minutes, allowing a better understanding of ambient sources of NPs.[8-10] Biomass or wood burning is a predominant contributor to the wintertime particle-phase NPs at levels of a few ng m^{-3} in the residential areas in UK and USA.[8,9] In an oil-gas-production region, secondary production has been identified as the main source of gaseous NPs.[10] In polluted urban environments, offline measurements show high concentrations of gaseous NPs up to several hundreds of ng m^{-3}.[11-13] Both primary and secondary contributions may be important because of the high anthropogenic

emissions (e.g., from the growing vehicle fleet) and strong oxidation capacity.[14,15] However, there is a lack of online measurements of NPs in urban areas. The formation and sources of gaseous NPs and their potential to produce OH in urban environments remain unclear.

In this study, we measured gaseous NPs by using the online nitrate-adduct ToF-CIMS (NO_3^--ToF-CIMS) in Beijing during the fall of 2016. Six classes of NPs are quantified, including nitrophenol (NPh), methylnitrophenol (MNP), dimethylnitrophenol or ethylnitrophenol (DMNP), dinitrophenol (DNP), nitrocatechol (NC), and methylnitrocatechol (MNC). Although isomers cannot be distinguished in these measurements, we evaluated the potential contributions of known formation and loss pathways to the concentration variations of gaseous NPs on the basis of precursor and oxidant concentrations. The results highlight the importance of secondary formation of NPs in maintaining the high production rates of NPs in urban environments.

EXPERIMENTAL METHODS

Measurements were conducted from 11 September 2016 to 4 October 2016 at an eight-floor roof site of the Peking University Urban Atmosphere Environment Monitoring Station (PKUERS). This site is located between the fourth and the fifth north ring roads in Beijing (39.99º N, 116.32º E, and 30 m above the ground), representing a typical urban environment influenced by various anthropogenic emissions.[16] Instrument operation and data analysis are provided in Sect. S1 of the Supporting Information (SI). Briefly, gaseous NPs were measured by the Aerodyne NO_3^--ToF-CIMS (Fig. S1 in SI). Volatile organic compounds (VOCs) were measured by an IONICON proton

transfer reaction-quadrupole interface time-of-flight mass spectrometer (PTR-QiToF).[17] The chemical composition of non-refractory $PM_{2.5}$ was measured by an Aerodyne time-of-flight aerosol chemical speciation monitor (ToF-ACSM) equipped with $PM_{2.5}$ aerodynamic lens and a capture vaporizer.[16] The concentrations of OH and NO_3 radicals herein were obtained from the measurements by a custom-built laser induced fluorescence instrument (LIF) and the measurements by a custom-built incoherent broadband cavity-enhanced absorption spectrometer (IBBCEAS), respectively.[18,19] The $PM_{2.5}$ mass concentrations were measured by a tapered element oscillating microbalance monitor (Thermo, TEOM 1400A). Atmospheric non-methane hydrocarbons (NMHCs, more than 50 VOC species) were measured by using a custom-built online gas chromatograph with mass spectrometer and flame ionization detector (GC-MS/FID).[20] NO-NO_x and O_3 were measured by trace gas analyzers (Thermo, 42i-TL and 49i-TL, respectively). Temperature, relative humidity (RH), wind speed, and wind direction were measured by a weather station (Met One, 083E-010C-020C).

The mass calibration of the CIMS spectra was performed on the reagent ions and selected fluorine-containing ions, including NO_3^-, $HNO_3 \cdot NO_3^-$, $C_2F_3O_2^-$, $C_2F_3HO_2 \cdot NO_3^-$, $(HNO_3)_2 \cdot NO_3^-$, and $C_{11}F_{21}H_3O_5 \cdot NO_3^-$, which covers the *m*/*z* range of 62 to 676. The fluorine-containing species were released from Teflon tubing used for delivering sheath flow. The mass accuracy for individual ions was less than 10 ppm for the whole campaign. Background signals from sheath flow and sampling line were determined by injecting zero air to the inlet periodically. The average background was subtracted from the measured signal intensities, which was about 9% for DNP

and 1-2% for the other five classes of NPs. The detection limits (DLs) of 0.05 to 0.9 ppt were estimated as three times of the standard deviation of the background signals for each classes of NPs (Table 1).

Details about the calibration and the quantification of NPs are described in the Sect. S2 of SI. Calibration experiments were performed on 2-nitrophenol, 4-nitrophenol, and 2-methyl-4-nitrophenol to determine the instrument sensitivities. For 2-nitrophenol, the calibration used liquid standards (Sigma-Aldrich, 98%). The standards were sampled through the heated filter inlet for gases and aerosols (FIGAERO) by high-purity nitrogen and sampled by the nitrate inlet. The calibration for 2-nitrophenol from the FIGAERO method, however, showed unstable baseline signals which affects the calculation of instrument sensitivity and thus was only used for qualitative analysis. The calibrations of 4-nitrophenol and 2-methyl-4-nitrophenol were conducted by sampling the standard gas from certificated permeation tubes (KinTek, about 100 ng min^{-1} at 100 °C) (Figs. S2-S4 in SI). Only the instrument sensitivity of 4-nitrophenol was applied to NPh, and the sensitivity of 2-methyl-4-nitrophenol was applied to the other NPs for quantification (Table 1).

Sampling-loss experiments were conducted by measuring the standard gas with or without the 90-cm sampling tube. The sampling loss was about 30% for 4-nitrophenol and about 23% for 2-methyl-4-nitrophenol. We applied an average sampling loss of 26% to all NPs. In addition, isotopically labelled nitric acid ($H^{15}NO_3$, Sigma-Aldrich, 40 wt. % in H_2O) was used as the reagent instead of nitric acid (HNO_3, Sigma-Aldrich, 70%) for ambient sampling for a short time. The

changes in the spectra when switching the reagent and the mass spectra of the calibration standards support the formula assignments of the NPs. The uncertainties of the quantification mainly consist of the errors in the peak fitting (<5%), the uncertainties in the concentration output and calibration curves of standard gas (10%), the representativeness of the calibrated species (<40%), and the uncertainties of the sampling losses (4%), which can be propagated to the overall uncertainties of about 42% for the NPs herein. In addition, we evaluated the production and the loss rates of NPs from known pathways on the basis of a Master Chemical Mechanism (MCM v3.3.1) based box model with concentration inputs of hydrocarbons and oxidants etc. Details about the budget analysis are provided in the Sect. S3 of SI.

RESULTS AND DISCUSSION

***Mass Concentrations*.** The mass spectra of standard samples confirm the detection of NPh and MNP by NO_3^--ToF-CIMS. NPs are predominantly detected as their clusters with NO_3^- (Fig. S2a). The ion formulas are determined first by the ion intensities of the adjacent isotope peaks and then the mass spectra of ambient air measured when using $H^{15}NO_3$ as the reagent for the ToF-CIMS (Sect. S2). The changes of the mass spectra after switching the reagent from HNO_3 to $H^{15}NO_3$ indicate that one of the two nitrogen atoms in the ion formulas must origin from the reagent ion, and the other one originates from the analyte molecule (Fig. S3). Their deprotonated ions and their clusters with $HNO_3 \cdot NO_3^-$ also present in the spectra. The intensities of the NO_3^--adduct ions are over 20 times more than the intensities of deprotonated and $HNO_3 \cdot NO_3^-$-adduct

ions for NPh and MNP, similar to the ambient spectra (Fig. S2b). Figure 1 shows the high-resolution peak fitting of the NO_3^--adduct ions that were used for the quantification of NPs. These ions are the dominant ions at each *m*/*z*, for which the peak fittings are less affected by isobaric ions unlike those in the spectra collected by the acetate-adduct ToF-CIMS.[10] Organic species that can be detected by NO_3^--ToF-CIMS are typically highly oxygenated with multifunctional groups, except for fluorine-containing ones or strong acids in the low *m*/*z* range (e.g., malonic acid). The highly selective detection of NPs by nitrate chemical ionization is perhaps because of their hydrogen-bond donor phenolic groups and the conjugation of the benzene ring with the nitro group.[21,22]

Figure 2 shows the concentration time series of gaseous NPs, $PM_{2.5}$, and organic aerosols (OA) during the measurement period as well as the meteorological parameters. The measurements are categorized into clean (< 35 μg m^{-3}) and haze (> 75 μg m^{-3}) days on the basis of the daily mean mass concentrations of $PM_{2.5}$. Severe haze days that have high $PM_{2.5}$ and OA concentrations are often associated with stagnant weather conditions.[23] The concentrations of NPs differ greatly by species and show large enhancements during the haze days compared with the clean days. All NPs except DNP show significant diurnal variations of the gas-phase concentrations, especially during the haze days.

Table 1 lists the mean concentrations of the six classes of NPs during the measurement periods. The observations in Beijing are generally consistent with the offline measurements in other large cities. NPh has the greatest campaign-average concentration of 238.2 ± 154.6 ng m^{-3} among the

six classes of NPs. The mean concentrations of NPh and DMNP are similar to those observed in Milan, Italy.[12] MNP has greater mean concentrations in Beijing than in other urban locations, whereas the concentrations of DNP are relatively lower in Beijing than in Santiago, Chile.[11-13,24] Quantitative gas-phase measurements for NC and MNC are limited. The study in Iowa City, USA reported a low concentration of less than 0.1 ng m^{-3}.[24] Their concentrations in Beijing ranged from 1.1 to 18.8 ng m^{-3}, which is 1-2 orders of magnitude greater than the concentrations in Iowa City. The higher NC and MNC may be explained by the large anthropogenic emissions in Beijing. On the other hand, compounds like phenyl or benzyl nitrates, methoxynitrobenzenes, nitroguaiacol, hydroxycarboxylic acids derived from pyridine, and nitrobenzyl alcohols have the same formulas as NPs. We cannot exclude the possible contribution of these molecules to the observed signals, although their atmospheric concentrations are expected to be lower than those of NPs because of limited primary sources.

The mean concentrations of NPh, MNP, DMNP, NC, and MNC for the haze days are about 1 to 2 times greater than their mean concentrations for the clean days. The haze-to-clean concentration ratio for DNP is high (i.e., 5.8), which is much greater than the haze-to-clean ratios of CO (1.9), NO_2 (1.8), and its precursor NPh (2.4). The result suggests that the haze conditions with high NPh and NO_x concentrations may favor the formation of DNP, possibly through aqueous reactions under conditions of relatively high aerosol liquid water content (ALWC).[25] Similar haze-to-clean concentration ratios are found for MNP and DMNP as well as NC and MNC. The time series of these two pair classes correlate strongly (Fig. 2e-f and Table S1 in SI), suggesting great

similarities in their precursors or formation pathways in polluted urban environments. The concentration ratios of MNP to DMNP and NC to MNC are 4.0 ± 1.0 and 1.7 ± 1.1, respectively.

Diurnal Variations and Sources. Figure 3 shows the diurnal variations of the concentrations of NPs. Diurnal profiles for clean and haze periods are similar to the profiles for the whole measurement period. All NPs except DNP exhibit daytime enhancements. The mixing ratios of NPh show two peaks, one at noon and the other at 6-7 p.m. The evening peak concentration is greater than the noon peak (Fig. 3a). The mixing ratios of MNP and DMNP peak around 5-6 p.m. (Fig. 3c-d), while NC and MNC peak around 1-2 p.m. (Fig. 3e-f). DNP had a relatively flattened diurnal profile with a nighttime peak occurring around 9 p.m. and a significant daytime reduction in concentration (Fig. 3b). The changing rates of gaseous NPs are calculated from their diurnal profiles as the derivatives of the mean concentrations with respect to time (ppt h^{-1}). Positive values of the changing rate mean net production rates, while negative values mean net loss rates. Various production and loss pathways as well as gas-particle partitioning may be involved and are discussed in the later subsection. NPh, MNP, and DMNP show persistent net production between 6 a.m. to 6 p.m. and otherwise net loss. Their maximum net production rates were 13.5, 5.4, and 1.2 ppt h^{-1}, respectively, and all occurred in the late afternoon (4:30-5:00 p.m.). By contrast, NC and MNC have shorter net production duration from 6 a.m. to 1 p.m. Their maximum net production rates are 0.4 and 0.3 ppt h^{-1}, respectively, which occurs in the morning (10:30-11:30 a.m.). For DNP, net production happens between 7:30 to 8:30 a.m. and 4:00 to 8:30 p.m. with a maximum net production rate of 1.8 ppt h^{-1} at 7 p.m., indicating insufficient production to outweigh

174 the mid-day photolysis loss.

175 Vehicle exhaust is a common primary source of NPs.[14,26] The concentration peaks in the
176 diurnal profiles of the NPs however do not match with the rush hours in Beijing (7-9 a.m. and 5-7
177 p.m.). The correlation coefficients (Pearson *r*) of the concentrations of the six NPs with NO are
178 lower than 0.14 (Table S2 in SI), suggesting that vehicle exhaust is unlikely the dominant source
179 of NPs in Beijing. Biomass burning episodically influences the air in Beijing by regional transport
180 in fall.[27] However, the concentration correlations between NPs and CH_3CN (i.e., a biomass burning
181 tracer measured by PTR-QiToF) are low for gaseous MNP, DMNP, NC and MNC ($r \leq 0.36$) and
182 moderate for NPh and DNP ($r \approx 0.5$) (Table S2). This is different from a previous study in Detling,
183 UK, which showed good correlations of biomass burning tracers with the particle-phase
184 concentrations of NPs.[8] In Beijing, biomass burning is likely one of the contributors but not a
185 dominant source of NPh and DNP during the measurement period. Coal combustion may
186 contribute significantly to NPs especially in winter when residential coal burning becomes an
187 important source.[7] In this study, the temporal correlations between NPs and naphthalene
188 (polycyclic aromatic hydrocarbon) are weak ($r \leq 0.41$), suggesting a minor primary contribution
189 of coal combustion to NPs during the measurement period (Table S2).

190 NPs can be produced secondarily by the gas-phase reactions of VOC precursors (e.g.,
191 aromatic compounds) with OH or NO_3 radicals in the presence of NO_2.[1,28] Yuan et al. show that
192 the gas-phase oxidation of aromatic compounds predominantly contributed to NPs in the oil-gas-
193 production region in the US.[10] The diurnal profiles of NPs in their study however show a daytime

194 concentration valley because of the strong photolysis loss. The concentrations of both oxidants
195 and precursors herein are several times greater than those reported by Yuan et al., indicating a
196 greater potential of secondary production of NPs in Beijing. Indeed, the diurnal profiles of all NPs
197 except DNP show clear daytime concentration enhancements. Figure S5 shows the diurnal profiles
198 of the concentrations of OH, NO_3, NO_2, and aromatic precursors such as phenol, cresol, benzene,
199 and toluene. The diurnal variations of phenolic precursors and oxidants as well as NO_2 are in
200 general consistent with the noontime and evening concentration peaks of NPs. The morning peaks
201 of phenol and cresol follow the rush-hour concentration peaks of benzene and toluene, which is
202 consistent with the secondary formation by OH addition. The high nighttime concentrations of
203 phenol and cresol may be caused by primary contributions of biomass burning or quantification
204 interferences by isomeric species (e.g., vinylfuran from biomass burning).[10,29-31] Consistently, the
205 nighttime concentrations of C_6H_6O correlates temporally with that of CH_3CN (Fig. S6 in SI). NPh
206 and DNP show good correlations with NO_2 (Table S2 in SI), which may be caused by increasing
207 NP yields from phenol and NPh oxidation for increasing NO_2 levels. Such influence of the NO_2
208 concentration has been reported previously in flow-tube experiments, although at unrealistic high
209 NO_2 levels.[32] The correlations of MNP, DMNP, NC and MNC with NO_2 are not as good as those
210 for NPh and DNP (Table S2 in SI), possibly because of the decreasing yields of catechol formed
211 from phenol oxidation for increasing NO_2 which were also previously found in flow-tube
212 experiments.[32] The diurnal profiles of NC and MNC indicate that their daytime production might
213 be greater than the nighttime production. Low yields of NC and MNC precursors (i.e., catechol

and methlycatechol) are expected in the evening because of the high NO_2 levels. Moreover, NPs can be potentially formed from the reaction of phenoxy radical with NO_2, and the phenoxy radical can be formed from the reaction of NO with phenyl peroxy radicals produced by a wide range of aromatic precursors. These reactions may lead to the noon and evening production of NPs (Fig. S7a-b in SI), which is consistent with our observations.

Nitration that happened in the aqueous phase of aerosol or cloud water is another secondary formation pathway of NPs. Box model analysis suggests that when the liquid water content (LWC) exceeds the volume fraction of 3×10^{-9}, the aqueous-phase nitration of phenol may contribute significantly to the production of NPh.[33] During the measurement period, particles likely appeared as liquid phase at the observed RH of 67.5 ± 18.3% because of the high concentrations of inorganic salts.[34] The ALWC was 24.7 ± 47.5 and 52.4 ± 65.7 μg m^{-3} (i.e., the volume fraction of 2.5×10^{-11} and 5.2×10^{-11}) for the clean and haze days, respectively, estimated by the reverse ISORROPIA model (Sect. S3). Such an amount of ALWC in Beijing is still limited to produce significant amount of NPs by the bulk aqueous-phase reactions, which is consistent with the poor correlation between the concentrations of the six NPs and the ALWC (Table S2 in SI).

Secondary Production and Photolysis Loss. To further investigate the secondary production of gaseous NPs, we conducted the budget analysis by comparing the observed changing rates with the calculated production and loss rates from the known production and loss pathways (Sect. S3). We mainly focus here on NPh and MNP because their concentrations were calibrated and their phenolic precursors were measured by the PTR-QiToF. The gas-phase chemical production is only

from the reaction of phenoxy or methylphenoxy radical ($C_6H_5O\cdot$ or $C_7H_7O\cdot$) + NO_2, while the $C_6H_5O\cdot$ or $C_7H_7O\cdot$ radicals are produced by the oxidation of phenol or cresol with OH and NO_3 radicals and by the reaction of phenyl peroxy radical ($C_6H_5O_2\cdot$) or methylphenyl peroxy radicals ($C_7H_7O_2\cdot$) with NO. Primary emissions and aqueous-phase production of NPh and MNP are plausibly minor contributors to the changing rates of NP concentrations and their potential influences are discussed qualitatively. The budget analysis was limited to daytime from 5 a.m. to 5 p.m. according to the diurnal profiles of the CH_3CN concentrations to minimize the potential influence of isomeric vinyl- and propyl-furans from biomass burning on the detection of phenol and cresol by the PTR-QiToF.[29-31] The downward mixing of the residual layer where the NPs production may be continued by NO_3 chemistry overnight may affect the NP concentrations in the morning, which is difficult to quantify. The loss pathways of gaseous NPs mainly consist of the chemical reactions of NPh and MNP with OH and NO_3 radicals, the physical losses due to dilution and deposition, and the photolysis. Gas-particle mass transfer varies by species and seasons (perhaps temperature matters)[25] and may also affect the gaseous concentrations of NPs, which will be discussed later.

Figure 4 shows the estimated production and loss rates compared with the observed changing rates of gaseous NPh and MNP. The observed net production rates are about several ppt h^{-1} for the two NPs during the day. The MCM box model predicts daytime maximum mean production rates of 113 and 62 ppt h^{-1} for NPh and MNP, respectively (Fig. 4c-d). The phenol/cresol + OH/NO_3 channels only accounts for a small fraction (< 10 ppt h^{-1}) of the production of $C_6H_5O\cdot$ and

254 $C_7H_7O\cdot$ radicals. The dominant production comes from the $C_6H_5O_2\cdot$ and $C_7H_7O_2\cdot$ + NO reactions
255 (Fig. S7a-b in SI), similar to the findings in the oil-gas-production region.[10] For the loss terms, the
256 chemical losses of NPh and MNP are minor contributors (< 3 ppt h^{-1}) (Fig. S7c-d). Physical loss
257 rates for atmospheric dilution and deposition are about 7-27×10^{-5} s^{-1}, corresponding to the
258 concentration loss rates of 7-43 and 3-18 ppt h^{-1} for NPh and MNP, respectively. Photolysis perhaps
259 contributes to the rest of the removal (Fig. 4e-f).

260 Photolysis has been recognized as a dominant sink for gaseous NPs.[1,3] There are however
261 limited measurements on the photolysis rates of NPs.[4,5] Bardini et al. reported a rate constant of
262 1.4% of the photolysis rate constant of NO_2 (J_{NO2}) for 2-nitrophenol in the EUPHORE chamber.[35]
263 Bejan et al. reported the photolysis rates of 3-methyl-2-nitrophenol, 4-methyl-2-nitrophenol, 5-
264 methyl-2-nitrophenol and 6-methyl-2-nitrophenol relative to J_{NO2} (3.9-8.4%) in a flow-tube photo-
265 reactor.[3] Sangwan et al. measured the wavelength-dependent absorption cross sections and
266 quantum yields for 2-nitrophenol, 4-methyl-2-nitrophenol, and 5-methyl-2-nitrophenol, which are
267 1-2 orders of magnitude greater than the relative photolysis rate constants reported by Bardini et
268 al. and Bejan et al. As expected, the calculated photolysis rates on the basis of the three studies
269 differ greatly (Fig. 4e-f). In comparison with the observation-constrained photolysis rates (i.e.,
270 modeled production rates – observed net changing rates – chemical and physical losses),
271 Sangwan's results are one order of magnitude greater, whereas Bejan and Bardini's findings are
272 2-10 times lower. The uncertainties of the modeled production rates, observed net changing rates,
273 and estimated chemical/physical losses are about 45%, 42%, and 66%, respectively, which

propagates to 90% of uncertainty for the observation-constrained photolysis rates.

The mass transfer by gas-particle partitioning may affect the gaseous concentrations. The calculated particle-phase proportion (F_p) on the basis of the partition theory and saturation vapor pressure are extremely low (10^{-4} to10^{-5}) for NPh and MNP. The measured F_p in China are however greater (i.e., 10-30% for NPh and MNP in spring and summer of 2016).[25,36] Wang et al.[37] reported a summertime mean particle-phase concentration of NPh+MNP of 3.7 ng m^{-3} in 2016 but at a different site in Beijing. With this value, we may obtain an F_p of 1.2%. Yang et al.[38] reported mean particle-phase concentrations of 20.5 ng m^{-3} for 4-NPh and 10 ng m^{-3} for 3-methyl-4-NPh from March 2016 to January 2017 in Beijing. With these values, we may obtain F_p values about 10% for this study, which seems more reasonable compared to other measurements of 10-30%. Nevertheless, the majority of NPh and MNP is expected to be in gas phase. The change of gaseous concentrations of NPh and MNP and consequently the change of net changing rate are still minor even with a complete particle to gas conversion as temperature rises, although such changes might be significant for other species (e.g., NC and MNC) that exist dominantly in the particle phase.[25] Besides, the physical loss rates estimated herein are greater than used in other NP studies.[10,39] Lower physical loss term may lead to greater observation-constrained photolysis rates. The magnitude of the observation-constrained photolysis rates is still determined by the modeled production rates. Therefore, the 90% uncertainty as well as the potential bias in physical loss estimates and gas-particle mass transfer cannot explain the large differences between these results and the photolysis rates measured in the laboratory. Unknown secondary formation mechanisms

294 are necessary to explain the data if Sangwan's wavelength-dependent measurements are more
295 accurate than the others. Moreover, an earlier morning peak exist in the observation-constrained
296 photolysis rates (Fig. 4e-f) at 7 a.m., which seems unreasonable. One explanation for this "fake"
297 photolysis is perhaps the contribution of the mixing down of the residual layer with high
298 concentrations of NPs.

299 **ATMOSPHERIC IMPLICATIONS**

300 In this study, high concentrations of gaseous NPs are observed in Beijing. The distinct diurnal
301 profiles of NPs that are different from those of primary emissions lead us to a conclusion that
302 secondary productions of NPs outweigh losses in urban Beijing. This conclusion is in line with the
303 high emissions of precursors, strong oxidative capacity, and high NO_x levels in polluted urban
304 environments. More importantly, we highlight the large discrepancy in current understanding of
305 the photolysis of gaseous NPs. Our results illustrate that the gas-phase photolysis of NPs perhaps
306 have a minor role in producing atmospheric oxidants in Beijing. Significantly underestimated
307 concentrations for OH radicals have been observed in closure studies in China with currently
308 available chemical mechanisms.[18,40-43] For instance, a study in a suburban site (Yufa) in Beijing
309 showed an underestimation of the OH production rate of 11 ppb h^{-1}.[44] Tan et al. reported peak OH
310 production rates of around 2 ppb h^{-1} from HONO photolysis, 1.2 ppb h^{-1} from O_3 photolysis, and
311 10 ppb h^{-1} from HO_2 recycling via NO reaction at a rural site (Wangdu) in the North China Plain
312 in summer.[18,45] The mean production rates of OH that are estimated from the observation-

313 constrained photolysis of NPh and MNP herein are about 0.08 and 0.05 ppb h^{-1}, respectively,
314 suggesting a total production rate of < 1 ppb h^{-1} for all NPs. This contribution is minor compared
315 with the underestimated OH production in urban environments. The NP-related OH production
316 that is calculated on the basis of Sangwan's results are one order of magnitude greater, which may
317 be significant but requires a large unknown secondary production source of NPs. Future studies
318 are needed to understand the gas-phase photolysis of NPs and ascertain the roles of NPs in oxidant
319 production in urban environments.
320
321 **ASSOCIATED CONTENT**
322 **Supporting Information**
323 This information is available free of charge on the ACS Publications website.
324 **AUTHOR INFORMATION**
325 **Corresponding Author**
326 *(Qi Chen) Phone: +86-10-62750508; e-mail: qichenpku@pku.edu.cn
327 **Notes**
328 The authors declare no competing financial interests.
329 **ACKNOWLEDGMENT**
330 This study was funded by the National Natural Science Foundation of China (41875165, 41675120,
331 41961134034, 51861135102), the 111 Project of Urban Air Pollution and Health Effects (B20009),
332 the Science and Technology Development Fund, Macau SAR (File no. 0019/2020/A1), the Multi-

333 Year Research grant of the University of Macau (No. MYRG2018-00006-FST), and the European
334 Research Council under the program CHAPAs (grant no. 850614)

335

336

REFERENCES

(1) Harrison, M. A. J.; Barra, S.; Borghesi, D.; Vione, D.; Arsene, C.; Olariu, R. L., *Nitrated phenols in the atmosphere: a review*, *Atmos. Environ.* **2005,** *39*, (2), 231-248.

(2) Bejan, I.; Abd El Aal, Y.; Barnes, I.; Benter, T.; Bohn, B.; Wiesen, P.; Kleffmann, J., *The photolysis of ortho-nitrophenols: a new gas phase source of HONO*, *Phys. Chem. Chem. Phys.* **2006,** *8*, (17), 2028-2035.

(3) Bejan, I.; Barnes, I.; Olariu, R.; Zhou, S.; Wiesen, P.; Benter, T., *Investigations on the gas-phase photolysis and OH radical kinetics of methyl-2-nitrophenols*, *Phys. Chem. Chem. Phys.* **2007,** *9*, (42), 5686-5692.

(4) Sangwan, M.; Zhu, L., *Absorption cross sections of 2-nitrophenol in the 295-400 nm region and photolysis of 2-nitrophenol at 308 and 351 nm*, *J. Phys. Chem. A* **2016,** *120*, (50), 9958-9967.

(5) Sangwan, M.; Zhu, L., *Role of methyl-2-nitrophenol photolysis as a potential source of OH radicals in the polluted atmosphere: implications from laboratory investigation*, *J. Phys. Chem. A* **2018,** *122*, (7), 1861-1872.

(6) Chow, K. S.; Huang, X. H. H.; Yu, J. Z., *Quantification of nitroaromatic compounds in atmospheric fine particulate matter in Hong Kong over 3 years: field measurement evidence for secondary formation derived from biomass burning emissions*, *Environ. Chem.* **2016,** *13*, (4), 665-673.

(7) Wang, L.; Wang, X.; Gu, R.; Wang, H.; Yao, L.; Wen, L.; Zhu, F.; Wang, W.; Xue, L.; Yang,

L.; Lu, K.; Chen, J.; Wang, T.; Zhang, Y.; Wang, W., *Observations of fine particulate nitrated phenols in four sites in northern China: concentrations, source apportionment, and secondary formation*, *Atmos. Chem. Phys.* **2018,** *18*, (6), 4349-4359.

(8) Mohr, C.; Lopez-Hilfiker, F. D.; Zotter, P.; Prevot, A. S. H.; Xu, L.; Ng, N. L.; Herndon, S. C.; Williams, L. R.; Franklin, J. P.; Zahniser, M. S.; Worsnop, D. R.; Knighton, W. B.; Aiken, A. C.; Gorkowski, K. J.; Dubey, M. K.; Allan, J. D.; Thornton, J. A., *Contribution of nitrated phenols to wood burning brown carbon light absorption in Detling, United Kingdom during winter time*, *Environ. Sci. Technol.* **2013,** *47*, (12), 6316-6324.

(9) Gaston, C. J.; Lopez-Hilfiker, F. D.; Whybrew, L. E.; Hadley, O.; McNair, F.; Gao, H. L.; Jaffe, D. A.; Thornton, J. A., *Online molecular characterization of fine particulate matter in Port Angeles, WA: evidence for a major impact from residential wood smoke*, *Atmos. Environ.* **2016,** *138*, 99-107.

(10) Yuan, B.; Liggio, J.; Wentzell, J.; Li, S. M.; Stark, H.; Roberts, J. M.; Gilman, J.; Lerner, B.; Warneke, C.; Li, R.; Leithead, A.; Osthoff, H. D.; Wild, R.; Brown, S. S.; de Gouw, J. A., *Secondary formation of nitrated phenols: insights from observations during the Uintah Basin Winter Ozone Study (UBWOS) 2014*, *Atmos. Chem. Phys.* **2016,** *16*, (4), 2139-2153.

(11) Cecinato, A.; Di Palo, V.; Pomata, D.; Sciano, M. C. T.; Possanzini, M., *Measurement of phase-distributed nitrophenols in Rome ambient air*, *Chemosphere* **2005,** *59*, (5), 679-683.

(12) Belloli, R.; Bolzacchini, E.; Clerici, L.; Rindone, B.; Sesana, G.; Librando, V., *Nitrophenols in air and rainwater*, *Environ. Eng. Sci.* **2006,** *23*, (2), 405-415.

(13) Rubio, M. A.; Lissi, E.; Herrera, N.; Perez, V.; Fuentes, N., *Phenol and nitrophenols in the air and dew waters of Santiago de Chile*, *Chemosphere* **2012,** *86*, (10), 1035-1039.

(14) Inomata, S.; Tanimoto, H.; Fujitani, Y.; Sekimoto, K.; Sato, K.; Fushimi, A.; Yamada, H.; Hori, S.; Kumazawa, Y.; Shimono, A.; Hikida, T., *On-line measurements of gaseous nitro-organic compounds in diesel vehicle exhaust by proton-transfer-reaction mass spectrometry*, *Atmos. Environ.* **2013,** *73*, 195-203.

(15) Lu, K.; Fuchs, H.; Hofzumahaus, A.; Tan, Z.; Wang, H.; Zhang, L.; Schmitt, S. H.; Rohrer, F.; Bohn, B.; Broch, S.; Dong, H.; Gkatzelis, G. I.; Hohaus, T.; Holland, F.; Li, X.; Liu, Y.; Liu, Y.; Ma, X.; Novelli, A.; Schlag, P.; Shao, M.; Wu, Y.; Wu, Z.; Zeng, L.; Hu, M.; Kiendler-Scharr, A.; Wahner, A.; Zhang, Y., *Fast photochemistry in wintertime haze: consequences for pollution mitigation strategies*, *Environ. Sci. Technol.* **2019,** *53*, (18), 10676-10684.

(16) Zheng, Y.; Cheng, X.; Liao, K. R.; Li, Y. W.; Li, Y. J.; Hu, W. W.; Liu, Y.; Zhu, T.; Chen, S. Y.; Zeng, L. M.; Worsnop, D.; Chen, Q.; Huang, R. J., *Characterization of anthropogenic organic aerosols by TOF-ACSM with the new capture vaporizer*, *Atmos. Meas. Tech.* **2020,** *13*, (5), 2457-2472.

(17) Huang, G.; Liu, Y.; Shao, M.; Li, Y.; Chen, Q.; Zheng, Y.; Wu, Z.; Liu, Y.; Wu, Y.; Hu, M.; Li, X.; Lu, S.; Wang, C.; Liu, J.; Zheng, M.; Zhu, T., *Potentially important contribution of gas-phase oxidation of naphthalene and methylnaphthalene to secondary organic aerosol during haze events in Beijing*, *Environ. Sci. Technol.* **2019,** *53*, (3), 1235-1244.

(18) Tan, Z. F.; Fuchs, H.; Lu, K. D.; Hofzumahaus, A.; Bohn, B.; Broch, S.; Dong, H. B.; Gomm,

S.; Haseler, R.; He, L. Y.; Holland, F.; Li, X.; Liu, Y.; Lu, S. H.; Rohrer, F.; Shao, M.; Wang, B. L.; Wang, M.; Wu, Y. S.; Zeng, L. M.; Zhang, Y. S.; Wahner, A.; Zhang, Y. H., *Radical chemistry at a rural site (Wangdu) in the North China Plain: observation and model calculations of OH, HO2 and RO2 radicals*, *Atmos. Chem. Phys.* **2017,** *17*, (1), 663-690.

(19) Wang, H. C.; Chen, J.; Lu, K. D., *Development of a portable cavity-enhanced absorption spectrometer for the measurement of ambient NO3 and N2O5: experimental setup, lab characterizations, and field applications in a polluted urban environment*, *Atmos. Meas. Tech.* **2017,** *10*, (4), 1465-1479.

(20) Wang, M.; Shao, M.; Chen, W.; Lu, S.; Liu, Y.; Yuan, B.; Zhang, Q.; Zhang, Q.; Chang, C. C.; Wang, B.; Zeng, L.; Hu, M.; Yang, Y.; Li, Y., *Trends of non-methane hydrocarbons (NMHC) emissions in Beijing during 2002-2013*, *Atmos. Chem. Phys.* **2015,** *15*, (3), 1489-1502.

(21) Hyttinen, N.; Kupiainen-Määttä, O.; Rissanen, M. P.; Muuronen, M.; Ehn, M.; Kurtén, T., *Modeling the charging of highly oxidized cyclohexene ozonolysis products using nitrate-based chemical ionization*, *J. Phys. Chem. A* **2015,** *119*, (24), 6339-6345.

(22) Hyttinen, N.; Otkjær, R. V.; Iyer, S.; Kjaergaard, H. G.; Rissanen, M. P.; Wennberg, P. O.; Kurtén, T., *Computational comparison of different reagent ions in the chemical ionization of oxidized multifunctional compounds*, *J. Phys. Chem. A* **2018,** *122*, (1), 269-279.

(23) An, Z.; Huang, R.-J.; Zhang, R.; Tie, X.; Li, G.; Cao, J.; Zhou, W.; Shi, Z.; Han, Y.; Gu, Z.; Ji, Y., *Severe haze in northern China: a synergy of anthropogenic emissions and atmospheric processes*, *Proc. Natl. Acad. Sci. U. S. A.* **2019,** *116*, (18), 8657-8666.

(24) Al-Naiema, I. M.; Stone, E. A., *Evaluation of anthropogenic secondary organic aerosol tracers from aromatic hydrocarbons*, *Atmos. Chem. Phys.* **2017,** *17*, (3), 2053-2065.

(25) Li, M.; Wang, X.; Lu, C.; Li, R.; Zhang, J.; Dong, S.; Yang, L.; Xue, L.; Chen, J.; Wang, W., *Nitrated phenols and the phenolic precursors in the atmosphere in urban Jinan, China*, *Sci. Total Environ.* **2020,** *714*, 136760.

(26) Sekimoto, K.; Inomata, S.; Tanimoto, H.; Fushimi, A.; Fujitani, Y.; Sato, K.; Yamada, H., *Characterization of nitromethane emission from automotive exhaust*, *Atmos. Environ.* **2013,** *81*, 523-531.

(27) Sun, Y. L.; Jiang, Q.; Xu, Y. S.; Ma, Y.; Zhang, Y. J.; Liu, X. G.; Li, W. J.; Wang, F.; Li, J.; Wang, P. C.; Li, Z. Q., *Aerosol characterization over the North China Plain: haze life cycle and biomass burning impacts in summer*, *J. Geophys. Res.* **2016,** *121*, (5), 2508-2521.

(28) Atkinson, R.; Aschmann, S. M.; Arey, J., *Reactions of OH and NO3 radicals with phenol, cresols, and 2-nitrophenol at 296 ± 2 K*, *Environ. Sci. Technol.* **1992,** *26*, (7), 1397-1403.

(29) Karl, T. G.; Christian, T. J.; Yokelson, R. J.; Artaxo, P.; Hao, W. M.; Guenther, A., *The tropical forest and fire emissions experiment: method evaluation of volatile organic compound emissions measured by PTR-MS, FTIR, and GC from tropical biomass burning*, *Atmos. Chem. Phys.* **2007,** *7*, (22), 5883-5897.

(30) Friedli, H. R.; Atlas, E.; Stroud, V. R.; Giovanni, L.; Campos, T.; Radke, L. F., *Volatile organic trace gases emitted from North American wildfires*, *Global. Biogeochem. Cy.* **2001,** *15*, (2), 435-452.

(31) Stockwell, C. E.; Veres, P. R.; Williams, J.; Yokelson, R. J., *Characterization of biomass burning emissions from cooking fires, peat, crop residue, and other fuels with high-resolution proton-transfer-reaction time-of-flight mass spectrometry*, *Atmos. Chem. Phys.* **2015,** *15*, (2), 845-865.

(32) Berndt, T.; Böge, O., *Gas-phase reaction of OH radicals with phenol*, *Phys. Chem. Chem. Phys.* **2003,** *5*, (2), 342-350.

(33) Harrison, M. A. J.; Heal, M. R.; Cape, J. N., *Evaluation of the pathways of tropospheric nitrophenol formation from benzene and phenol using a multiphase model*, *Atmos. Chem. Phys.* **2005,** *5*, 1679-1695.

(34) Liu, Y. C.; Wu, Z. J.; Huang, X. F.; Shen, H. Y.; Bai, Y.; Qiao, K.; Meng, X. X. Y.; Hu, W. W.; Tang, M. J.; He, L. Y., *Aerosol phase state and its link to chemical composition and liquid water content in a subtropical coastal megacity*, *Environ. Sci. Technol.* **2019,** *53*, (9), 5027-5033.

(35) Bardini, P., *Atmospheric chemistry of dimethylphenols & nitrophenols*, *Ph.D. thesis, University College Cork.* **2006,** *1*, (1), 1–156.

(36) Le Breton, M.; Wang, Y. J.; Hallquist, A. M.; Pathak, R. K.; Zheng, J.; Yang, Y. D.; Shang, D. J.; Glasius, M.; Bannan, T. J.; Liu, Q. Y.; Chan, C. K.; Percival, C. J.; Zhu, W. F.; Lou, S. R.; Topping, D.; Wang, Y. C.; Yu, J. Z.; Lu, K. D.; Guo, S.; Hu, M.; Hallquist, M., *Online gas- and particle-phase measurements of organosulfates, organosulfonates and nitrooxy organosulfates in Beijing utilizing a FIGAERO ToF-CIMS*, *Atmos. Chem. Phys.* **2018,** *18*, (14), 10355-10371.

(37) Wang, Z. H.; Zhang, J. Y.; Zhang, L. Z.; Liang, Y. M.; Shi, Q., *Characterization of*

nitroaromatic compounds in atmospheric particulate matter from Beijing, *Atmos. Environ.* **2021,** *246*.

(38) Yang, Y.; Li, X. R.; Shen, R. R.; Liu, Z. R.; Ji, D. S.; Wang, Y. S., *Seasonal variation and sources of derivatized phenols in atmospheric fine particulate matter in North China Plain*, *J Environ Sci* **2020,** *89*, 136-144.

(39) Salvador, C. M. G.; Tang, R. Z.; Priestley, M.; Li, L. J.; Tsiligiannis, E.; Le Breton, M.; Zhu, W. F.; Zeng, L. M.; Wang, H.; Yu, Y.; Hu, M.; Guo, S.; Hallquist, M., *Ambient nitro-aromatic compounds - biomass burning versus secondary formation in rural China*, *Atmos. Chem. Phys.* **2021,** *21*, (3), 1389-1406.

(40) Lou, S.; Holland, F.; Rohrer, F.; Lu, K.; Bohn, B.; Brauers, T.; Chang, C. C.; Fuchs, H.; Haeseler, R.; Kita, K.; Kondo, Y.; Li, X.; Shao, M.; Zeng, L.; Wahner, A.; Zhang, Y.; Wang, W.; Hofzumahaus, A., *Atmospheric OH reactivities in the Pearl River Delta - China in summer 2006: measurement and model results*, *Atmos. Chem. Phys.* **2010,** *10*, (22), 11243-11260.

(41) Lu, K. D.; Rohrer, F.; Holland, F.; Fuchs, H.; Bohn, B.; Brauers, T.; Chang, C. C.; Haeseler, R.; Hu, M.; Kita, K.; Kondo, Y.; Li, X.; Lou, S. R.; Nehr, S.; Shao, M.; Zeng, L. M.; Wahner, A.; Zhang, Y. H.; Hofzumahaus, A., *Observation and modelling of OH and HO2 concentrations in the Pearl River Delta 2006: a missing OH source in a VOC rich atmosphere*, *Atmos. Chem. Phys.* **2012,** *12*, (3), 1541-1569.

(42) Tan, Z.; Rohrer, F.; Lu, K.; Ma, X.; Bohn, B.; Broch, S.; Dong, H.; Fuchs, H.; Gkatzelis, G. I.; Hofzumahaus, A.; Holland, F.; Li, X.; Liu, Y.; Liu, Y.; Novelli, A.; Shao, M.; Wang, H.; Wu, Y.;

Zeng, L.; Hu, M.; Kiendler-Scharr, A.; Wahner, A.; Zhang, Y., *Wintertime photochemistry in Beijing: observations of ROx radical concentrations in the North China Plain during the BEST-ONE campaign*, *Atmos. Chem. Phys.* **2018,** *18*, (16), 12391-12411.

(43) Tan, Z.; Lu, K.; Hofzumahaus, A.; Fuchs, H.; Bohn, B.; Holland, F.; Liu, Y.; Rohrer, F.; Shao, M.; Sun, K.; Wu, Y.; Zeng, L.; Zhang, Y.; Zou, Q.; Kiendler-Scharr, A.; Wahner, A.; Zhang, Y., *Experimental budgets of OH, HO2, and RO2 radicals and implications for ozone formation in the Pearl River Delta in China 2014*, *Atmos. Chem. Phys.* **2019,** *19*, (10), 7129-7150.

(44) Lu, K. D.; Hofzumahaus, A.; Holland, F.; Bohn, B.; Brauers, T.; Fuchs, H.; Hu, M.; Häseler, R.; Kita, K.; Kondo, Y.; Li, X.; Lou, S. R.; Oebel, A.; Shao, M.; Zeng, L. M.; Wahner, A.; Zhu, T.; Zhang, Y. H.; Rohrer, F., *Missing OH source in a suburban environment near Beijing: observed and modelled OH and HO2 concentrations in summer 2006*, *Atmos. Chem. Phys.* **2013,** *13*, (2), 1057-1080.

(45) Tan, Z.; Lu, K.; Jiang, M.; Su, R.; Wang, H.; Lou, S.; Fu, Q.; Zhai, C.; Tan, Q.; Yue, D.; Chen, D.; Wang, Z.; Xie, S.; Zeng, L.; Zhang, Y., *Daytime atmospheric oxidation capacity in four Chinese megacities during the photochemically polluted season: a case study based on box model simulation*, *Atmos. Chem. Phys.* **2019,** *19*, (6), 3493-3513.

Table 1. The quantification parameters and the concentrations of gaseous NPs measured by the NO_3^--ToF-CIMS in comparison with other urban measurements.

Species Name: Ions for quantification	*m/z*		Instrument Sensitivity (ncps ppt^{-1})	DLs (ppt)	Gas-phase Concentrations (ng m^{-3})				
	Exact Mass	Error (ppm)			Clean[a]	Haze[a]	Whole Campaign[a]	5th – 95th Percentiles	Reference Mean[f]
NPh: $(C_6H_5NO_3)NO_3^-$	201.0153	-3.98	0.0020	0.9	137±80	331±151	238±155	48.1~520	14.3[b] 256[c] 499[d]
MNP: $(C_7H_7NO_3)NO_3^-$	215.0310	-5.12	0.0013	0.5	39.7±28.1	94.4±55.0	71.0±54.5	16.0~181	13.9[b] 17.3[c] 5.3[e]
DMNP: $(C_8H_9NO_3)NO_3^-$	229.0466	-3.06	0.0013	0.2	13.7±14.7	28.4±18.4	21.6±19.3	4.1~60.1	2.0[b] 24.3[c]
DNP: $(C_6H_4N_2O_5)NO_3^-$	246.0004	2.03	0.0013	0.9	13.5±18.3	78.2±65.9	42.8±53.5	8.2~181	224[d]
NC: $(C_6H_5NO_4)NO_3^-$	217.0102	3.69	0.0013	0.05	6.3±5.0	8.1±5.4	7.3±5.4	1.4~18.8	0.09[e]
MNC: $(C_7H_7NO_4)NO_3^-$	231.0259	-8.22	0.0013	0.07	4.5±3.1	6.1±3.9	5.5±3.8	1.1~13.4	0.08[e]

[a]Mean ± 1 standard deviation of the concentrations.
[b]Downtown Rome, Italy (Cecinato et al.[11]).
[c]Urban Milan, Italy (Belloli et al.[12]).
[d]Downtown Santiago, Chile (Rubio et al.[13]).
[e]Iowa City, IA, USA (Al-Naiema and Stone[24]).
[f]Represent the summed concentrations of detected isomers.

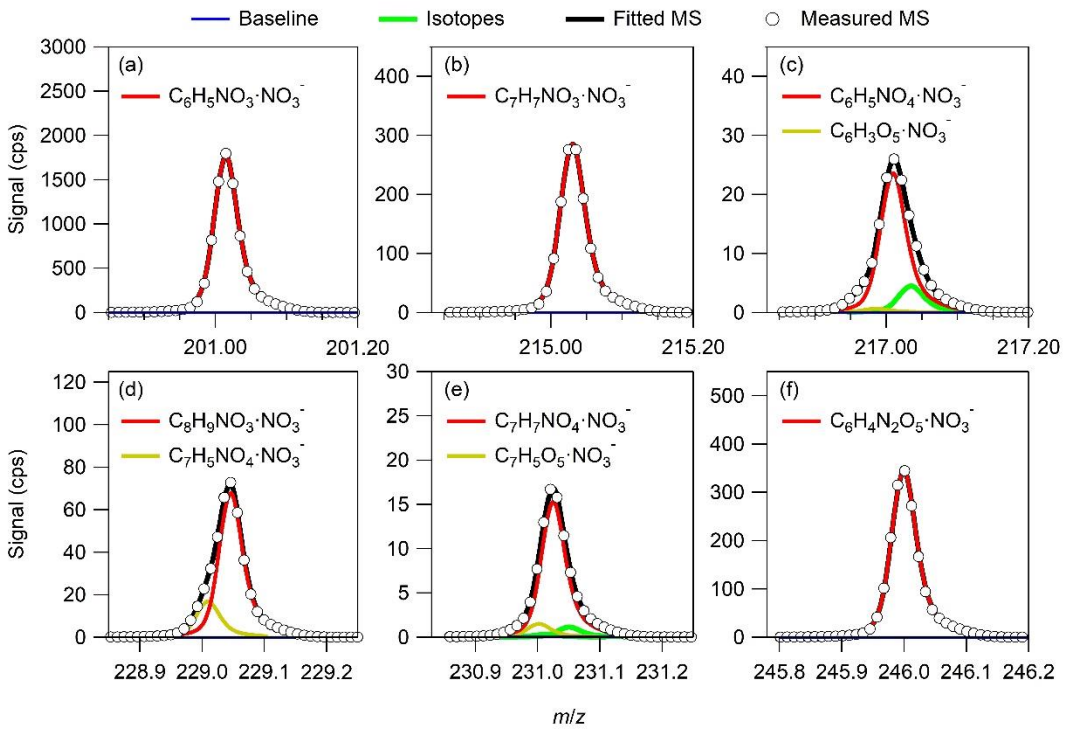

Figure 1. High-resolution peak fitting to the average mass spectra obtained by the NO_3^--ToF-CIMS for (a) *m*/*z* 201, (b) *m*/*z* 215, (c) *m*/*z* 217, (d) *m*/*z* 229, (e) *m*/*z* 231, and (f) *m*/*z* 246 on 1 October 2016 in Beijing.

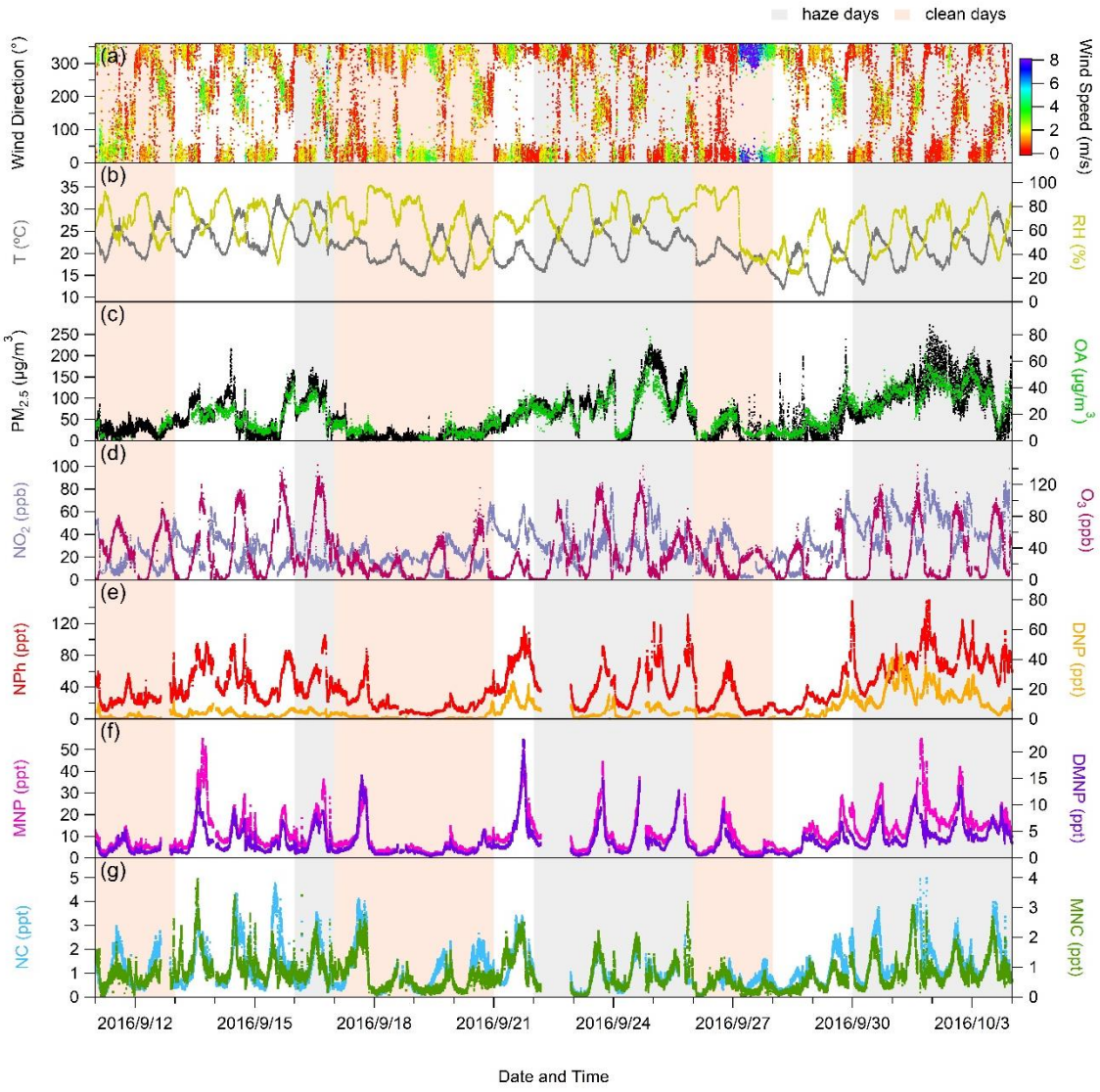

Figure 2. Time series of (a) wind direction and wind speed, (b) temperature and RH, (c) the mass concentrations of $PM_{2.5}$ and OA, (d) the mixing ratios of NO_2 and O_3, and (e-g) the mixing ratios of the six classes of NPs measured by NO_3^--ToF-CIMS.

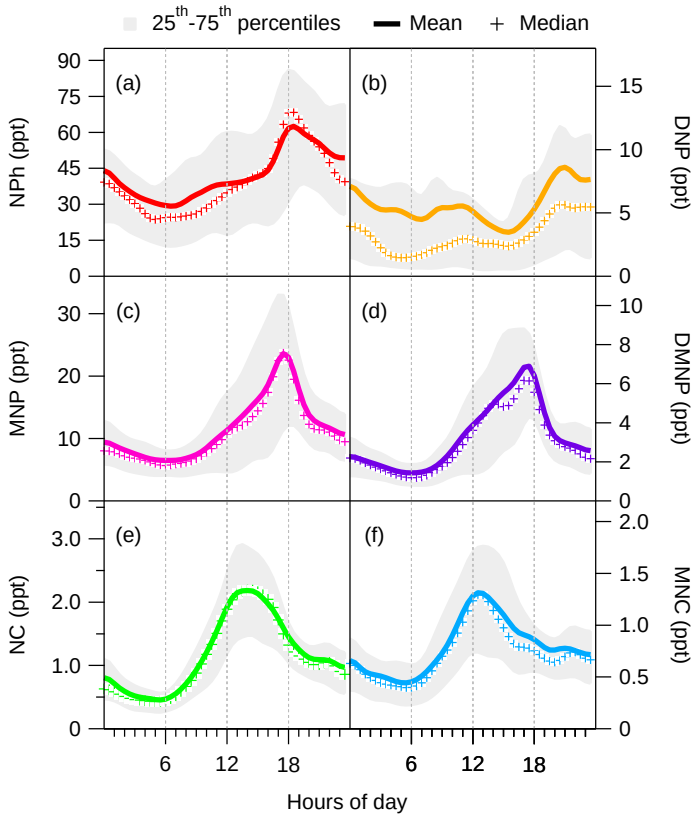

Figure 3. Diurnal profiles of the concentrations of (a) NPh, (b)DNP, (c) MNP, (d) DMNP, (e) NC, (f) MNC for the whole measurement period. The shaded areas represent the 25th and 75th percentiles. The mean and median curves are smoothed by the binomial Gaussian filter with a smoothing factor of 3.

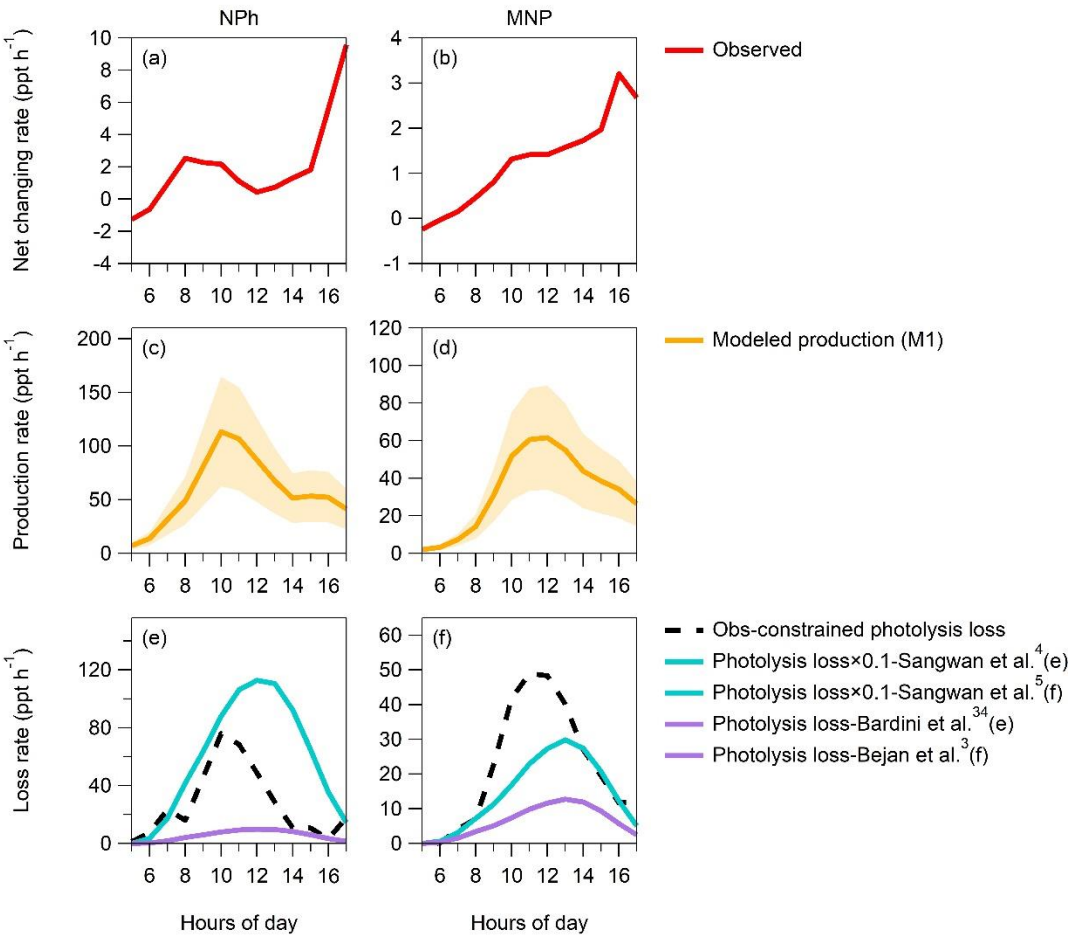

Figure 4. Mean diurnal profiles of the observed net changing rates (a, b), the modeled production rates (c, d), and constrained photolysis loss rates (e, f) for NPh and MNP. Modeled production rates are calculated by MCM v3.3.1 and the shaded area shows the roughly estimated uncertainty of 45%. The observation constrained photolysis loss rates are calculated by subtracting the observed net changing rates, chemical losses, and the physical losses of NPh and MNP from the modeled production rates. The constrained photolysis rates are compared to the photolysis loss rates from literature.

Supporting Information for

Secondary Production of Gaseous Nitrated Phenols in Polluted Urban Environments

Xi Cheng,[1] Qi Chen,[1,] Yongjie Li,[2] Guancong Huang,[1] Ying Liu,[1] Sihua Lu,[1] Yan Zheng,[1] Wanyi Qiu,[1] Keding Lu,[1] Xinghua Qiu,[1] Federico Bianchi,[3] Chao Yan,[3,4] Bin Yuan,[5] Min Shao,[1,5] Zhe Wang,[6] Manjula R. Canagaratna,[7] Tong Zhu,[1] Yusheng Wu,[1] Limin Zeng[1]*

[1]State Key Joint Laboratory of Environmental Simulation and Pollution Control, BIC-ESAT and IJRC, College of Environmental Sciences and Engineering, Peking University, Beijing, China

[2]Department of Civil and Environmental Engineering, Faculty of Science and Technology, University of Macau, Taipa, Macau, China

[3]Institute for Atmospheric and Earth System Research, Faculty of Science, University of Helsinki, Helsinki, Finland

[4]Aerosol and Haze Laboratory, Beijing Advanced Innovation Center for Soft Matter Science and Engineering, Beijing University of Chemical Technology, Beijing, China

[5]Institute for Environmental and Climate Research, Jinan University, Guangzhou, China

[6]Division of Environment and Sustainability, The Hong Kong University of Science and Technology, Hong Kong, China

[7]Aerodyne Research Inc., Billerica, MA, USA

***Correspondence to:**

Qi Chen (Email: qichenpku@pku.edu.cn)

This file includes:

Supporting Text Section S1, S2, S3

Supporting Table S1, S2, S3

Supporting Figure S1-S11

Number of pages: 33

S1. Instrument Operation and Data Analysis

NO_3^--ToF-CIMS. The instrument consists of a chemical ionization (CI) at ambient pressure and a time-of-flight mass spectrometer (ToF-MS).[1] Nitric acid vapors (1-3 sccm) are diluted in the sheath flow and then are ionized by a soft X-ray ionization source. The sheath flow and the ambient air flow through the CI inlet in a laminar form. Nitrate ions in the sheath flow move towards the sample flow in an electric field. The charging of the sample air takes place at ambient pressure by collisions with nitrate clusters, $(HNO_3)_x \cdot NO_3^-$ (x = 0-2). The ionized air then enters the ToF-MS through a 0.3-mm pinhole with a flow rate of about 0.8 L min^{-1}. Highly acidic gases like sulfuric acid are detected as de-protonated ions and cluster ions (e.g., HSO_4^- and $HNO_3 \cdot HSO_4^-$ etc.).[1] Oxidized organic gases are typically detected as their clusters with NO_3^-. Their clusters with $HNO_3NO_3^-$ may also be detected depending on the availability of $HNO_3NO_3^-$.[2]

During the campaign, air was sampled through a 0.9-m, ¾ inch (outside diameter, O.D.) electro-polished stainless steel tube straight out of the window at the roof-top site. The sample flow rate was of 10 L min^{-1}. The sheath flow was supplied by zero air with a flow rate of 25 L min^{-1}. Zero air was injected in front of the inlet periodically for 20 to 30 min to determine the background. The instrument was tuned to maximize the signal ratio of $HNO_3NO_3^-$ to NO_3^- with good peak shape and mass resolution. It was operated for an *m*/*z* range of 1 to 1009 Th. The mass resolution was approximately 5000 for ions of *m*/*z* greater than 200. Mass spectra were saved for every second and were post-averaged to 1-minute for calculating the concentrations. Data were analyzed in Tofware (version 2.5.10), a WaveMetrics Igor toolkit package. Figure S1 shows the

average full mass spectra of whole campaign for the *m*/*z* range of 195-485. Peaks related to nitrated phenols (NPs) contribute predominantly to the total signals detected by NO_3^--ToF-CIMS. We quantified six classes of NPs herein (Table 1). Details about the quantification is described in Sect. S2.

PTR-QiToF. Volatile organic compounds (VOCs) were measured by using a proton transfer reaction-quadrupole interface time-of-flight mass spectrometer (PTR-QiToF). The instrument setup has been described previously by Huang et al.[3] Briefly, the drift tube of the PTR-QiTOF was operated at 3.8 mbar and 80 °C to reach an optimized sensitivity (1000-5000 ncps ppb^{-1}) and mass resolution (~6000). Mass spectra were collected at the time resolution of 10 s. Ambient air was sampled through an 8-m, ¼ inch (O.D.) polyfluoroalkoxy (PFA) tube with a flow rate of 8 L min^{-1}. For every 4 h, 25-min background signals were measured by switching ambient air through a platinum catalytic converter at 370 °C. Aromatics, acids, carbonyls, and phenols were calibrated by using gas standards (Spectra Gases, ~1 ppm) and certificated permeation tubes (KinTek) at five concentration levels from 0.5 to 20 ppb. For uncalibrated species, the quantification was based on the established transmission curve. Wall losses on Teflon tubing were estimated to be 5% for VOCs and 5-25% for IVOCs.[3] In this study, the concentrations of benzene (C_6H_6), toluene (C_7H_8), naphthalene ($C_{10}H_8$), phenol (C_6H_6O), cresol (C_7H_8O) and acetonitrile (CH_3CN) were used.

Other instruments. The chemical composition of non-refractory $PM_{2.5}$ was measured by an Aerodyne time-of-flight aerosol chemical speciation monitor (ToF-ACSM). This instrument was equipped with $PM_{2.5}$ aerodynamic lens and a capture vaporizer. The instrument setup has been

described previously by Zheng et al.[4] The ToF-ACSM data have 2-min time resolution and were processed in Tofware (Tofwerk version 2.5.13). A collection efficiency of 1 was applied. Calibrations of ionization efficiency (IE) and relative IE of the ToF-ACSM followed the standard procedures by using 300-350 nm pure NH_4NO_3 and $(NH_4)_2SO_4$. The temperature and pressure during calibration were 293.7 K and 101.82 KPa, which represent the reference conditions of mass concentrations reported herein. The OH radicals were measured by a laser-induced fluorescence system (LIF) at a 6-floor roof site of the Peking University Urban Atmosphere Environment Monitoring Station (PKUERS). The instrument setup was the same as described by Tan et al.[5] The uncertainty was about 14%. The concentations of NO_3 radicals were calculated from the thermodynamic equilibrium on the basis of the measurements by the custom-built incoherent broadband cavity enhanced absorption spectrometer (IBBCEAS). The instrument setup and data processing were described by Wang et al.[6] Other instruments including the tapered element oscillating microbalance monitor (Thermo, TEOM 1400A), trace-gas analyzers for NO-NO_2-NO_x (Thermo, 42i-TL) and ozone (Thermo, 49i-TL), and the weather station (Met One, 083E, 010C, 020C) were also installed in the 6-floor roof site, which is about 10 meters away from the 8-floor roof site.

S2. Quantification of NPs

The concentrations of NPs were calculated as follows:

$$[\mathrm{NP}] = \left(\frac{I_{\mathrm{NP}} - \overline{I_{\mathrm{NP,\,background}}}}{I_{NO_3^-} + I_{HNO_3NO_3^-} + I_{HNO_3HNO_3NO_3^-}}\right)\frac{1}{(1-\beta)S_{\mathrm{NP}}} \quad (1)$$

where *I*, β, and *S* represent the ion intensity (counts per second, cps), the fraction of sampling losses (%), and the instrument sensitivity (ncps ppt^{-1}), respectively. The signals of each NP were corrected for its own mean background (i.e., about 9% for DNP and 1-2% for other NPs) and then were normalized to the total signals of the reagent ions (normalized counts per second, ncps). The instrument sensitivity and the sampling losses were determined by the calibration experiments.

The NO_3^--ToF-CIMS for calibration was set-up in the same way as for ambient sampling. Calibrations of NPs were conducted after the campaign by two different methods. For 2-nitrophenol, the liquid standard was diluted in acetone. A series of samples was extracted by a micro-syringe (10-50 μL, corresponding to 15-76 ppt) and was deposited on the Teflon filter inside the filter inlet for gases and aerosols (FIGAERO). Gas sampling in the FIGAERO module was blocked. The Teflon filter was heated to 200 ℃ with a carrier gas of high-purity nitrogen of 2 L min^{-1}. The sample flow then mixed with a zero-air flow of 8 L min^{-1} to ensure the total flow of 10 L min^{-1} before entering the CI inlet. The signals of tracer ions were integrated over time per injection. For 4-nitrophenol and 2-methyl-4-nitrophenol, certificated permeation tubes (KinTek, 97 and 102 ng min^{-1} at 100 °C, respectively) were placed in the heated chamber at 100 ℃ in a calibration gas generator (VICI, Dynacalibrator 500). The calibration gas vapors were swept by a small flow of zero air and further diluted by a large flow of zero air. Then, 10 L min^{-1} of the standard gas flow was sampled by the NO_3^--ToF-CIMS. The signals of tracer ions gradually became stable after an initial stage. Five-point calibrations were repeated twice between 10 to 60 ppt for the two NPs.

NPs are predominantly detected as their clusters with NO_3^-. The deprotonated ions and the clusters with $HNO_3 \cdot NO_3^-$ present, but their intensities are much less than the intensities of their clusters with NO_3^-. Figure S3 shows the signals of *m*/*z* 201-203 for the mass spectra of ambient air and the fitted peaks when $H^{15}NO_3$ was used as the reagent to sample the ambient air in Beijing. When using HNO_3 as the reagent, the signals of *m*/*z* 202 and 203 were mainly contributed by the isotope peaks of the ion formula of $C_6H_5N_2O_6^-$ at *m*/*z* 201. After replacing the regent to $H^{15}NO_3$, the signals of reagent ions from HNO_3 were still strong because of the sticky background. The actual reagent in this case was a mixture of HNO_3 and $H^{15}NO_3$. The signal enhancement at *m*/*z* 202 and 203 indicated that one nitrogen was from NO_3^- in the formula of $C_6H_5N_2O_6^-$. This means that the ion at *m*/*z* 201 was $(C_6H_5NO_3)NO_3^-$ and the ions at *m*/*z* 202 were $(C_6H_5NO_3)^{15}NO_3^-$ and the isotope peak of $(C_6H_5NO_3)NO_3^-$, which support the assignments of the ion formulas of the six NPs herein. Figure S2a shows the mass spectra of the calibration standards. Figure S2b shows the NP-ions of the campaign-average mass spectra of ambient air measured in this study. The intensities of the deprotonated ions are over 20 times less than those of the NO_3^--adduct ions for nitrophenol (NPh), methylnitrophenol (MNP), and dimethylnitrophenol or ethylnitrophenol (DMNP). For nitrocatechol (NC), methylnitrocatechol (MNC), and dinitrophenol (DNP), the intensities of the deprotonated ions are comparable to the intensities of the NO_3^--adduct ions. Nevertheless the spectra confirmed the presence of ions from the NPs. In this study, the quantification of NPs was based on the NO_3^--adduct ions.

Figure S4 shows the calibration curves of the NO_3^--adduct ions of 4-nitrophenol and 2-methyl-4-nitrophenol measured by the NO_3^--ToF-CIMS. Good linearity was found for the two NPs calibrated by permeation tubes. The instrument sensitivity of 2-methyl-4-nitrophenol is 0.0013 ncps ppt^{-1}, which is less than the sensitivities of 4-nitrophenol (0.0020 ncps ppt^{-1}). For the calibration of 2-nitrophenol conducted by the FIGAERO method, we were unable to flush all the material into the system to obtain a good baseline per injection in a time scale of hours. The signal baseline kept rising up perhaps because of the repartitioning of 2-nitrophenol in the sampling line. The FIGAERO- NO_3^--ToF-CIMS setup has longer and narrower sampling line than the permeation-tube method. It is difficult to determine of the integration period for each injection. The derived instrument sensitivity was associated with a large uncertainty and therefore was not used. In this study, we used the sensitivity of 4-nitrophenol only to calculate the concentrations of NPh. The sensitivity of 2-methyl-4-nitrophenol was applied to other NPs (MNP, DMNP, NC, MNC, and DNP).

For acetate-adduct ToF-CIMS, the instrument sensitivities for 2-methyl-4-nitrophenol, 2,5-dinitrophenol, 2-nitrophenol, and 4-nitrophenol were reported as 16.6 ncps ppt^{-1}, 10.3 ncps ppt^{-1}, 8.4 ncps ppt^{-1}, and 18.0 ncps ppt^{-1}, respectively.[7] The sensitivities for 2- and 4-nitrophenol differ by over 50% in the study of Yuan et al.[7] Offline analysis in Milan shows similar concentrations of 2- and 4-nitrophenol in the urban air, while more studies shows dominant contribution of 4-nitrophenol. Taking into account the relative contributions, the uncertainty of using the sensitivity of 4-nitrophenol to calculate the NPh concentrations is estimated as less than 40%. Mohr et al.

(2013) showed the instrument sensitivities of 2.6×10^4 counts ng^{-1} for 4-nitrocatechol and 4×10^4 counts ng^{-1} for 4-methyl-2-nitrophenol.[8] The difference between NC, DNP, and MNP was also less than 40%. For our NO_3^--ToF-CIMS, the sensitivities of the standard NPs (i.e., $1\text{-}2\times10^{10}$ molecules·cm^{-3}) and H_2SO_4 (i.e., 0.9×10^{10} molecules·cm^{-3}) are similar, suggesting a minor change of sensitivity over *m*/*z* or chemical formula. We therefore expect an overall uncertainty of the representativeness of the calibrated species of < 40%.

In addition, experiments for determining the sampling losses of the NPs were conducted during the calibration of 4-nitrophenol at 27.6 ppt and 2-methyl-4-nitrophenol at 49.7 ppt. The standard gas was sampled through the 0.9-m ambient sampling tube. Sampling losses of 4-nitrophenol and 2-methyl-4-nitrophenol were estimated by the ratio of the signals of standard gas sampled with the ambient sampling tube to the signals of standard gas sampled directly by the CI inlet. The sampling losses were about 30% for 4-nitrophenol and 23% for 2-methyl-4-nitrophenol. In this study, we applied an average sampling loss fraction (β) of 26% for the six NPs.

The uncertainties of the quantification were mainly originated from the errors in the peak fitting (1-5% for the associated ions), the uncertainties in the concentration output and calibration curves of standard gas (10%), the representativeness of the calibrated species (<40%), and the uncertainties of the sampling losses (4%), which propagated to the overall uncertainties of about 42% for the NPs. The NP adduct ions detected by NO_3^--ToF-CIMS are the dominant ions at each *m*/*z*, for which the peak fittings are less affected by isobaric ions unlike those in the spectra collected by the acetate-adduct ToF-CIMS. The calibration factor of NPs is also similar to the

commonly-used calibration factors of H_2SO_4 and perfluoroheptanoic acid, indicating efficient clustering of NPs with nitrate ions. The highly selective detection of NPs by nitrate chemical ionization is perhaps because of their hydrogen-bond donor phenolic groups and the conjugation of the benzene ring with the nitro group. Similar to NO_3^--ToF-CIMS, iodide adduct detection of NPs is also sensitive, and the NP adduct clusters are the dominant ions.[9] The sampling wall losses of NPs for iodide-CIMS have however not yet been well characterized, which might be large because of the long sampling line.

S3. Calculation of the production and loss of NPs

Aerosol liquid water content (ALWC). The ALWC contributed by inorganic species such as ammonium, sulfate, nitrate, and chloride was estimated by a thermodynamic model ISORROPIA-II.[10] The model was run in the reverse mode with the assumption of stable state. The contribution of organic components to ALWC was estimated by assuming a hygroscopicity parameter of OA of 0.1.[11]

Phase transfer from gas-particle partitioning. Gas-particle partitioning of NPs greatly changed with species and seasons.[12] In this study, the concentration of NPs in particle phase were not measured. The NPs generated through gas-phase reactions would partition into particle-phase, leading to the gaseous losses of NPs. Here, the gas-particle partitioning of NPs was predicted using the absorption partitioning model, based on Eq. (2) and Eq. (3).

$$C^* = \frac{M10^6\zeta P_v}{RT} \quad (2)$$

$$F_p = \left(1 + \frac{C^*}{C_{OA}}\right)^{-1} \quad (3)$$

where C^* (μg·m^{-3}) is the effective saturation mass concentration, a key factor to influence the modelled F_p (the fraction of a species in the particle phase), C_{OA} (μg·m^{-3}) is the organic aerosol mass concentration measured from ToF-ACSM, M is the molecular weight (g·mol^{-1}), ζ is the activity coefficient in aerosol phase (here assumed to be unity), R is the gas constant (8.2 ×10^{-5} m^3·atm·K^{-1}·mol^{-1}), T is the temperature (K), and P_V (atm) is the sub-cooled liquid vapor pressure of NPs. The sub-cooled liquid vapor pressures of NPs were calculated using the University of Manchester (UManSysProp) online property prediction tool, which is based on the vapor pressure method[13] and the boiling point method.[14]

The saturation concentrations of NPh and MNP are about 1.1-5.0×10^5 μg m^{-3}, estimated by using the University of Manchester online property prediction tool (UManSysProp).[13,14] The mass concentrations of organic aerosol (OA) during the campaign ranged from 5 to 60 μg m^{-3} (Fig. 2). On the basis of partition theory, the mass fraction of particle-phase NPh and MNP are low (e.g., 2-NPh: 4.2 × 10^{-5}; 4-NPh: 6.6 × 10^{-5}; 2-methyl-6-NPh: 1.9×10^{-4}; 4-methyl-2-NPh: 1.9×10^{-4}). Even if particles become liquid, the aerosol aqueous-phase fractions of NPs are still low given the low Henry's law constants.[15] The measured F_p in China are however greater. For example, Salvador et al.[9] reported measured F_p of 9% for NPh and 12% for MNP in winter of 2017-2018 in Shandong, China. Le Breton et al.[16] found F_p of 17% for NPh in spring of 2016 at a suburban site nearby Beijing. Li et al.[12] reported F_p of ~30% for 4-NPh and ~20% for 3-methyl-4NPh and 2-methyl-4-NPh in summer of 2016 in Jinan, China.

By using our mean gaseous concentrations and the summertime mean particle-phase concentrations of NPh+MNP (3.7 ng m^{-3}) measured by Wang et al.[17] in the same year but at a different site in Beijing, we can obtain a mean F_p of 1.2%. If the mean particle-phase concentrations measured by Yang et al.[18] from Mar 2016 to Jan 2017 (i.e., 20.5 ng m^{-3} of 4-NPh and 10 ng m^{-3} of 3-methyl-4-NPh) are used, F_p values can be in 8 for NPh and 12% for MNP. With these F_p values, the 100% of mass transfer of the particle-phase NPh and MNP to the gas phase during the daytime as temperature rises would lead to roughly 10% of change in the gaseous concentrations. This may affect the net changing rate to some extent.

Physical loss. The nighttime physical loss rates caused by dilution and deposition at night were estimated from the first-order reduction rates of the NPh and MNP concentrations between 12 a.m. and 5 a.m. during the clean days when the chemical loss and source contributions were low (Fig. S8).[7,20] The fitted nighttime loss rates are (6.6 ± 6.7) and (13 ± 19)×10^{-5} s^{-1} for NPh and MNP, respectively. The daytime physical loss rates are difficult to determine. In September, the local CO source in Beijing is mainly vehicle emissions.[21] We may use the maximum daytime first-order reduction rates of CO (fitted to the data from 11 a.m. to 2 p.m.) to roughly constrain the daytime physical loss rate of NPs, which is (27 ± 18)×10^{-5} s^{-1}. When propagating uncertainties for the observation-constrained photolysis rates, 66% of uncertainty for the physical loss rate was used. For comparison, Salvador et al.[9] used physical loss rates of 9.3×10^{-5} s^{-1} and 2.8×10^{-4} s^{-1} for NC measured in another city in China in their model evaluation. Yuan et al.[7] estimated the physical loss rates of NPh (i.e., nighttime: 5.8×10^{-6} s^{-1}; daytime: 2.0×10^{-5} s^{-1}). We have used relatively large

physical loss rates herein. The physical loss was about 30-40% in the subtraction from production to constrain the peak photolysis rates (Fig. S7 and Fig. 4e-f). Lower physical loss rates may lead to greater obs-constrained photolysis rates but would not affect their magnitudes since their magnitudes are determined by the production rates (45% of uncertainty). The discussion about photolysis loss would not be affected much by the potential bias of physical losses.

Photolysis. Photolysis is an important removal pathway for gaseous NPs. The photolysis rate constants of NPs are calculated using the following equation:

$$J = \Sigma\, \sigma(\lambda)\varphi(\lambda)F(\lambda)\Delta\lambda \quad (4)$$

where J is the photolysis rate (s^{-1}). The J values depends on the absorption cross section $\sigma(\lambda)$ (cm^2), the quantum yield $\varphi(\lambda)$ at wavelength λ of the given molecule (the sum of the OH and HONO quantum yields), and the solar actinic flux $F(\lambda)$ that can be estimated by using the NCAR Tropospheric Ultraviolet-Visible (TUV) radiative transfer model. The measured photolysis rates of NO_2 (J_{NO_2}) were used to quantify the solar actinic flux and to derive the photolysis rates of NPs on the basis of the relative photolysis rate constants to J_{NO_2} reported by Bejan et al. and Bardini et al.[22,23] The maximum J_{NO_2} during the measurement period is 5×10^{-3} s^{-1}. We used the cross sections and the lower limits of photolysis quantum yields for 2-nitrophenol, 4-methyl-2-nitrophenol and 5- methyl-2-nitrophenol reported by Sangwan et al. to derive the photolysis rates of NPs herein.[24,25] After all, we applied the photolysis rate constant of 2-nitrophenol to NPh and the average value of the photolysis rate constants of methyl-2-nitrophenol isomers for MNP for these three studies.

Gas-phase reactions. The kinetic data for the gas-phase reactions are taken from the Master Chemical Mechanism (MCM v3.3.1) (http://mcm.leeds.ac.uk). Table S3 lists the rate coefficients of the reactions related to NPh and MNP. For the NPh/MNP formation, their loss rates were determined from NPh/MNP + OH and NPh/MNP + NO_3, which can be calculated on the basis of our measurements. The production rates of NPh and MNP were determined based on the reaction of phenoxy/methylphenoxy radical (RO·, i.e., C_6H_5O· and C_7H_7O·) + NO_2. The intermediate RO· were formed through the reactions of phenol/cresol + OH/NO_3, and the reactions of the RO_2· ($C_6H_5O_2$· and $C_7H_7O_2$·) + NO. Therefore, the variations of RO· (C_6H_5O· and C_7H_7O·) concentration is essential to calculate the production rates of NPh and MNP. Due to the lack of the observations of RO· (C_6H_5O· and C_7H_7O·), their concentrations were simulated with a zero-dimensional box model containing MCM v3.3.1 mechanisms.

The model inputs include the measured concentrations of VOCs, CO, NO, NO_2, O_3, as well as temperature, relative humidity, pressure, and the photolysis frequencies. VOCs were measured by using an online gas chromatograph mass spectrometer (GC-MS) during 23-31 August along with the PTR-QiToF measurements. Dry deposition rate for all modeled species is set to 1.2 cm s^{-1}.[26,27] The model is operated with 3 days spin-up time to reach steady state. The time step of the model calculation is set to 1 hour. M0 is the base case model with the settings described above. In another model scenario (M1), the measured phenol and cresol concentrations by PTR-QiToF are included as constraints to the model run. The models well reproduce OH and NO_3 radical chemistry. Figure S9 shows the time series and diurnal profiles of the OH and NO_3 concentrations. The diurnal

cycles of modeled OH and NO_3 radical are similar in shape to the measurements, although the measurements were conducted at other specific periods. Moreover, the modeled OH is compared with the calculated OH from the empirical OH-J_{O^1D} relations according to Lu et al.,[28] the difference is acceptable considering the fitting error between OH and J_{O^1D}. Model performance is evaluated by comparing the measured and modeled concentrations of phenol and cresol (Fig. S10). Generally, M0 reproduce the trends of phenol/cresol. The major difference appears at night is probably because of the primary emissions and the interference of primary emissions to PTR-QiToF measurements. The model uncertainty is estimated by the error propagation from all considered parameters (VOCs, trace gas, meteorological parameters, etc.) and the overall uncertainty is estimated to be around 45%.[27] Figure S11 shows the modeled RO· (C_6H_5O· and C_7H_7O·) concentration. Little difference present between M0 and M1 results during the day. Herein, the modeled concentrations from M1 have been used for calculating the production rates of NPh and MNP.

References

(1) Jokinen, T.; Sipilä, M.; Junninen, H.; Ehn, M.; Lönn, G.; Hakala, J.; Petäjä, T.; Mauldin Iii, R. L.; Kulmala, M.; Worsnop, D. R., *Atmospheric sulphuric acid and neutral cluster measurements using CI-APi-TOF*, *Atmos. Chem. Phys.* **2012,** *12*, (9), 4117-4125.

(2) Ehn, M.; Thornton, J. A.; Kleist, E.; Sipila, M.; Junninen, H.; Pullinen, I.; Springer, M.; Rubach, F.; Tillmann, R.; Lee, B.; Lopez-Hilfiker, F.; Andres, S.; Acir, I. H.; Rissanen, M.; Jokinen, T.; Schobesberger, S.; Kangasluoma, J.; Kontkanen, J.; Nieminen, T.; Kurten, T.; Nielsen, L. B.; Jorgensen, S.; Kjaergaard, H. G.; Canagaratna, M.; Dal Maso, M.; Berndt, T.; Petaja, T.; Wahner, A.; Kerminen, V. M.; Kulmala, M.; Worsnop, D. R.; Wildt, J.; Mentel, T. F., *A large source of low-volatility secondary organic aerosol*, *Nature* **2014,** *506*, (7489), 476-479.

(3) Huang, G.; Liu, Y.; Shao, M.; Li, Y.; Chen, Q.; Zheng, Y.; Wu, Z.; Liu, Y.; Wu, Y.; Hu, M.; Li, X.; Lu, S.; Wang, C.; Liu, J.; Zheng, M.; Zhu, T., *Potentially important contribution of gas-phase oxidation of naphthalene and methylnaphthalene to secondary organic aerosol during haze events in Beijing*, *Environ. Sci. Technol.* **2019,** *53*, (3), 1235-1244.

(4) Zheng, Y.; Cheng, X.; Liao, K. R.; Li, Y. W.; Li, Y. J.; Hu, W. W.; Liu, Y.; Zhu, T.; Chen, S. Y.; Zeng, L. M.; Worsnop, D.; Chen, Q.; Huang, R. J., *Characterization of anthropogenic organic aerosols by TOF-ACSM with the new capture vaporizer*, *Atmos. Meas. Tech.* **2020,** *13*, (5), 2457-2472.

(5) Tan, Z.; Rohrer, F.; Lu, K.; Ma, X.; Bohn, B.; Broch, S.; Dong, H.; Fuchs, H.; Gkatzelis, G. I.; Hofzumahaus, A.; Holland, F.; Li, X.; Liu, Y.; Liu, Y.; Novelli, A.; Shao, M.; Wang, H.; Wu,

Y.; Zeng, L.; Hu, M.; Kiendler-Scharr, A.; Wahner, A.; Zhang, Y., *Wintertime photochemistry in Beijing: observations of ROx radical concentrations in the North China Plain during the BEST-ONE campaign*, *Atmos. Chem. Phys.* **2018,** *18*, (16), 12391-12411.

(6) Wang, H. C.; Chen, J.; Lu, K. D., *Development of a portable cavity-enhanced absorption spectrometer for the measurement of ambient NO3 and N2O5: experimental setup, lab characterizations, and field applications in a polluted urban environment*, *Atmos. Meas. Tech.* **2017,** *10*, (4), 1465-1479.

(7) Yuan, B.; Liggio, J.; Wentzell, J.; Li, S. M.; Stark, H.; Roberts, J. M.; Gilman, J.; Lerner, B.; Warneke, C.; Li, R.; Leithead, A.; Osthoff, H. D.; Wild, R.; Brown, S. S.; de Gouw, J. A., *Secondary formation of nitrated phenols: insights from observations during the Uintah Basin Winter Ozone Study (UBWOS) 2014*, *Atmos. Chem. Phys.* **2016,** *16*, (4), 2139-2153.

(8) Mohr, C.; Lopez-Hilfiker, F. D.; Zotter, P.; Prevot, A. S. H.; Xu, L.; Ng, N. L.; Herndon, S. C.; Williams, L. R.; Franklin, J. P.; Zahniser, M. S.; Worsnop, D. R.; Knighton, W. B.; Aiken, A. C.; Gorkowski, K. J.; Dubey, M. K.; Allan, J. D.; Thornton, J. A., *Contribution of nitrated phenols to wood burning brown carbon light absorption in Detling, United Kingdom during winter time*, *Environ. Sci. Technol.* **2013,** *47*, (12), 6316-6324.

(9) Salvador, C. M. G.; Tang, R. Z.; Priestley, M.; Li, L. J.; Tsiligiannis, E.; Le Breton, M.; Zhu, W. F.; Zeng, L. M.; Wang, H.; Yu, Y.; Hu, M.; Guo, S.; Hallquist, M., *Ambient nitro-aromatic compounds - biomass burning versus secondary formation in rural China*, *Atmos. Chem. Phys.* **2021,** *21*, (3), 1389-1406.

(10) Nenes, A.; Pandis, S. N.; Pilinis, C., *ISORROPIA: a new thermodynamic equilibrium model for multiphase multicomponent inorganic aerosols*, *Aquatic Geochemistry* **1998,** *4*, (1), 123-152.

(11) Nguyen, T. K. V.; Zhang, Q.; Jimenez, J. L.; Pike, M.; Carlton, A. G., *Liquid water: ubiquitous contributor to aerosol mass*, *Environ. Sci. Technol. Let.* **2016,** *3*, (7), 257-263.

(12) Li, M.; Wang, X.; Lu, C.; Li, R.; Zhang, J.; Dong, S.; Yang, L.; Xue, L.; Chen, J.; Wang, W., *Nitrated phenols and the phenolic precursors in the atmosphere in urban Jinan, China*, *Sci. Total Environ.* **2020,** *714*, 136760.

(13) Nannoolal, Y.; Rarey, J.; Ramjugernath, D., *Estimation of pure component properties - part 3. estimation of the vapor pressure of non-electrolyte organic compounds via group contributions and group interactions*, *Fluid Phase Equilib.* **2008,** *269*, (1-2), 117-133.

(14) Nannoolal, Y.; Rarey, J.; Ramjugernath, D.; Cordes, W., *Estimation of pure component properties: part 1. estimation of the normal boiling point of non-electrolyte organic compounds via group contributions and group interactions*, *Fluid Phase Equilib.* **2004,** *226*, 45-63.

(15) Sander, R., *Compilation of Henry's law constants (version 4.0) for water as solvent*, *Atmos. Chem. Phys.* **2015,** *15*, (8), 4399-4981.

(16) Le Breton, M.; Wang, Y. J.; Hallquist, A. M.; Pathak, R. K.; Zheng, J.; Yang, Y. D.; Shang, D. J.; Glasius, M.; Bannan, T. J.; Liu, Q. Y.; Chan, C. K.; Percival, C. J.; Zhu, W. F.; Lou, S. R.; Topping, D.; Wang, Y. C.; Yu, J. Z.; Lu, K. D.; Guo, S.; Hu, M.; Hallquist, M., *Online gas- and particle-phase measurements of organosulfates, organosulfonates and nitrooxy organosulfates in Beijing utilizing a FIGAERO ToF-CIMS*, *Atmos. Chem. Phys.* **2018,** *18*, (14), 10355-10371.

(17) Wang, Z. H.; Zhang, J. Y.; Zhang, L. Z.; Liang, Y. M.; Shi, Q., *Characterization of nitroaromatic compounds in atmospheric particulate matter from Beijing*, *Atmos. Environ.* **2021,** *246*.

(18) Yang, Y.; Li, X. R.; Shen, R. R.; Liu, Z. R.; Ji, D. S.; Wang, Y. S., *Seasonal variation and sources of derivatized phenols in atmospheric fine particulate matter in North China Plain*, *J Environ Sci* **2020,** *89*, 136-144.

(19) Wang, Y.; Hu, M.; Wang, Y.; Zheng, J.; Shang, D.; Yang, Y.; Liu, Y.; Li, X.; Tang, R.; Zhu, W.; Du, Z.; Wu, Y.; Guo, S.; Wu, Z.; Lou, S.; Hallquist, M.; Yu, J. Z., *The formation of nitro-aromatic compounds under high NOx and anthropogenic VOC conditions in urban Beijing, China*, *Atmos. Chem. Phys.* **2019,** *19*, (11), 7649-7665.

(20) Wang, Z.; Yuan, B.; Ye, C.; Roberts, J.; Wisthaler, A.; Lin, Y.; Li, T.; Wu, C.; Peng, Y.; Wang, C.; Wang, S.; Yang, S.; Wang, B.; Qi, J.; Wang, C.; Song, W.; Hu, W.; Wang, X.; Xu, W.; Ma, N.; Kuang, Y.; Tao, J.; Zhang, Z.; Su, H.; Cheng, Y.; Wang, X.; Shao, M., *High concentrations of atmospheric isocyanic acid (HNCO) produced from secondary sources in China*, *Environ. Sci. Technol.* **2020,** *54*, (19), 11818-11826.

(21) Hao, J. M.; Wu, Y.; Fu, L. X.; He, D. Q.; He, K. B., *Source contributions to ambient concentrations of CO and NOx in the urban area of Beijing*, *J Environ Sci Health* **2001,** *36*, (2), 215-228.

(22) Bejan, I.; Barnes, I.; Olariu, R.; Zhou, S.; Wiesen, P.; Benter, T., *Investigations on the gas-phase photolysis and OH radical kinetics of methyl-2-nitrophenols*, *Phys. Chem. Chem. Phys.* **2007,**

9, (42), 5686-5692.

(23) Bardini, P., *Atmospheric chemistry of dimethylphenols & nitrophenols, Ph.D. thesis, University College Cork.* **2006,** *1*, (1), 1–156.

(24) Sangwan, M.; Zhu, L., *Absorption cross sections of 2-nitrophenol in the 295-400 nm region and photolysis of 2-nitrophenol at 308 and 351 nm, J. Phys. Chem. A* **2016,** *120*, (50), 9958-9967.

(25) Sangwan, M.; Zhu, L., *Role of methyl-2-nitrophenol photolysis as a potential source of OH radicals in the polluted atmosphere: implications from laboratory investigation, J. Phys. Chem. A* **2018,** *122*, (7), 1861-1872.

(26) Li, X.; Rohrer, F.; Brauers, T.; Hofzumahaus, A.; Lu, K.; Shao, M.; Zhang, Y. H.; Wahner, A., *Modeling of HCHO and CHOCHO at a semi-rural site in southern China during the PRIDE-PRD2006 campaign, Atmos. Chem. Phys.* **2014,** *14*, (22), 12291-12305.

(27) Liu, Y.; Yuan, B.; Li, X.; Shao, M.; Lu, S.; Li, Y.; Chang, C. C.; Wang, Z.; Hu, W.; Huang, X.; He, L.; Zeng, L.; Hu, M.; Zhu, T., *Impact of pollution controls in Beijing on atmospheric oxygenated volatile organic compounds (OVOCs) during the 2008 Olympic Games: observation and modeling implications, Atmos. Chem. Phys.* **2015,** *15*, (6), 3045-3062.

(28) Lu, K. D.; Hofzumahaus, A.; Holland, F.; Bohn, B.; Brauers, T.; Fuchs, H.; Hu, M.; Häseler, R.; Kita, K.; Kondo, Y.; Li, X.; Lou, S. R.; Oebel, A.; Shao, M.; Zeng, L. M.; Wahner, A.; Zhu, T.; Zhang, Y. H.; Rohrer, F., *Missing OH source in a suburban environment near Beijing: observed and modelled OH and HO2 concentrations in summer 2006, Atmos. Chem. Phys.* **2013,** *13*, (2), 1057-1080.

Table S1. Pearson correlation coefficients (*r*) for the correlations between the concentrations of individual NP for the measurement period.

	NPh	MNP	DMNP	DNP	NC	MNC
NPh	1					
MNP	0.78	1				
DMNP	0.65	0.89	1			
DNP	0.69	0.42	0.29	1		
NC	0.48	0.63	0.69	0.24	1	
MNC	0.53	0.60	0.70	0.20	0.75	1

Table S2. The *r* values for the correlations of the concentrations of NPs with gaseous tracers, OA, aerosol liquid water content (ALWC) for the measurement period.

	NPh	MNP	DMNP	DNP	NC	MNC
NO	0.00	-0.06	-0.11	0.14	-0.15	-0.12
NO_x	0.40	0.24	0.14	0.54	-0.02	0.05
NO_2	0.61	0.41	0.30	0.70	0.09	0.18
O_3	0.25	0.45	0.46	-0.04	0.58	0.38
CH_3CN	0.53	0.36	0.21	0.48	0.04	0.09
$C_{10}H_8$	0.32	0.03	-0.04	0.41	-0.20	-0.05
OA	0.76	0.51	0.40	0.73	0.24	0.31
ALWC	0.10	-0.06	-0.09	0.03	-0.22	-0.10

Table S3. Gas-phase reactions for NPh and MNP and their corresponding rate coefficients at 298 K, all taken from MCM v3.3.1.

Reaction	Rate coefficient ($cm^3 \cdot molecule^{-1} \cdot s^{-1}$)
$Phenol + OH \rightarrow C_6H_5O\cdot$	1.69×10^{-12}
$Phenol + NO_3 \rightarrow C_6H_5O\cdot$	2.82×10^{-12}
$C_6H_5O_2\cdot + NO \rightarrow C_6H_5O\cdot$	9.04×10^{-12}
$C_6H_5O_2\cdot + NO_3 \rightarrow C_6H_5O\cdot$	2.30×10^{-12}
$C_6H_6O_2 \rightarrow C_6H_5O\cdot$ (photolysis)	/
$C_6H_5O\cdot + NO_2 \rightarrow C_6H_5NO_3$	2.08×10^{-12}
$C_6H_5NO_3 + OH \rightarrow C_6H_4NO_3\cdot$	9.00×10^{-13}
$C_6H_5NO_3 + NO_3 \rightarrow C_6H_4NO_3\cdot$	9.00×10^{-14}
$Cresol + OH \rightarrow C_7H_7O\cdot$	3.39×10^{-12}
$Cresol + NO_3 \rightarrow C_7H_7O\cdot$	5.47×10^{-12}
$C_7H_7O_2\cdot + NO \rightarrow C_7H_7O\cdot$	9.04×10^{-12}
$C_7H_7O_2\cdot + NO_3 \rightarrow C_7H_7O\cdot$	2.30×10^{-12}
$C_7H_8O_2 \rightarrow C_7H_7O\cdot$ (photolysis)	/
$C_7H_7O\cdot + NO_2 \rightarrow C_7H_7NO_3$	2.08×10^{-12} 3.90×10^{-13}
$C_7H_7NO_3 + OH \rightarrow C_7H_6NO_3\cdot$	2.80×10^{-12}
$C_7H_7NO_3 + OH \rightarrow C_7H_8NO_8\cdot$	3.60×10^{-12}
$C_7H_7NO_3 + NO_3 \rightarrow C_7H_6NO_3\cdot$	3.13×10^{-13}

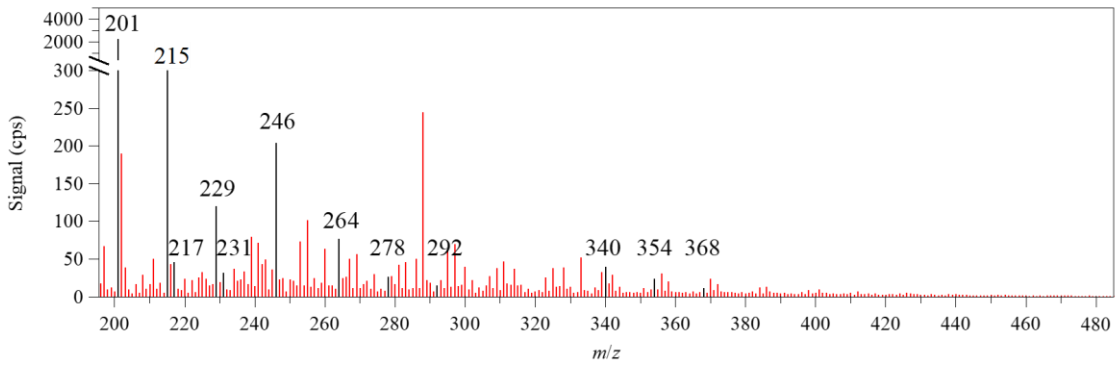

Figure S1. Average mass spectra detected by the NO_3^--ToF-CIMS during this campaign. Black lines represent the peaks related to NPs. Red lines represent the highly oxygenated organic molecules detected by NO_3^--ToF-CIMS.

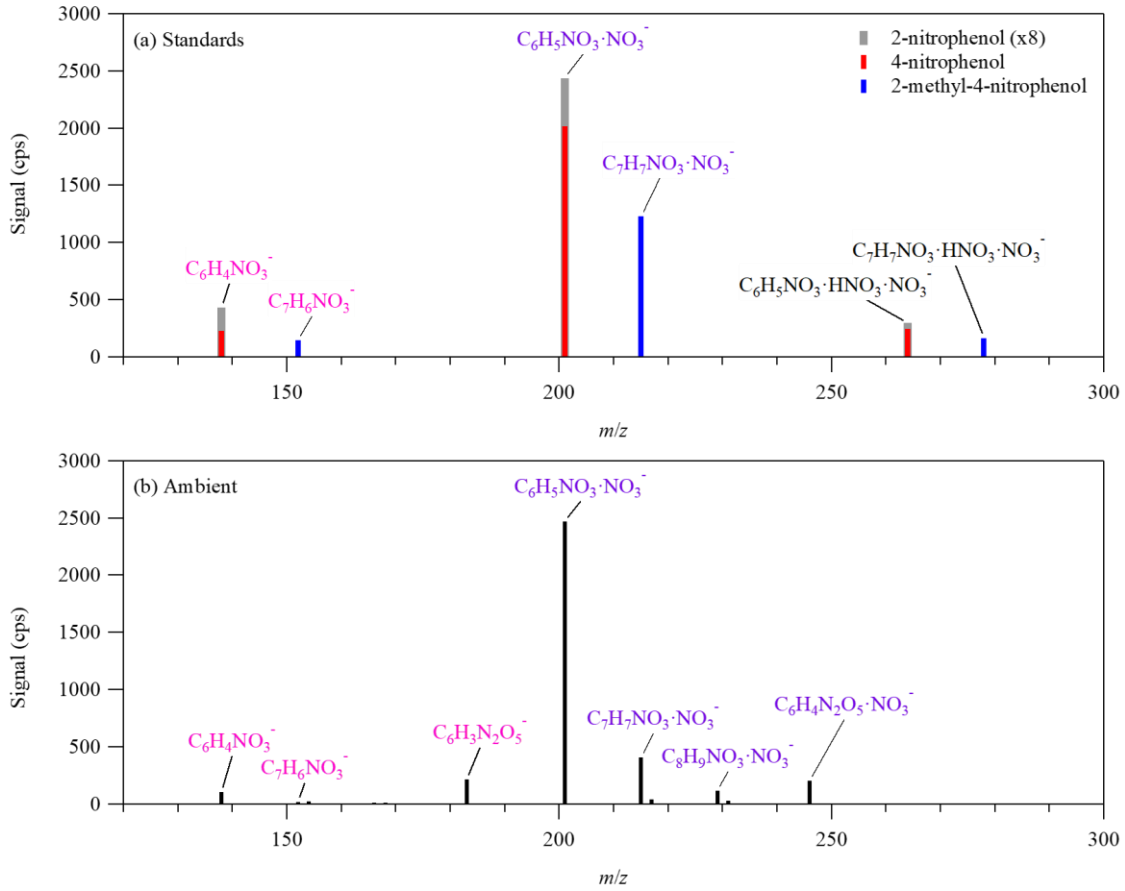

Figure S2. (a) Mass spectra of the calibration standards. (b) The campaign-average mass spectrum of ambient air in Bejing in a logarithmic scale. Only the ions of NPs are shown in both panels.

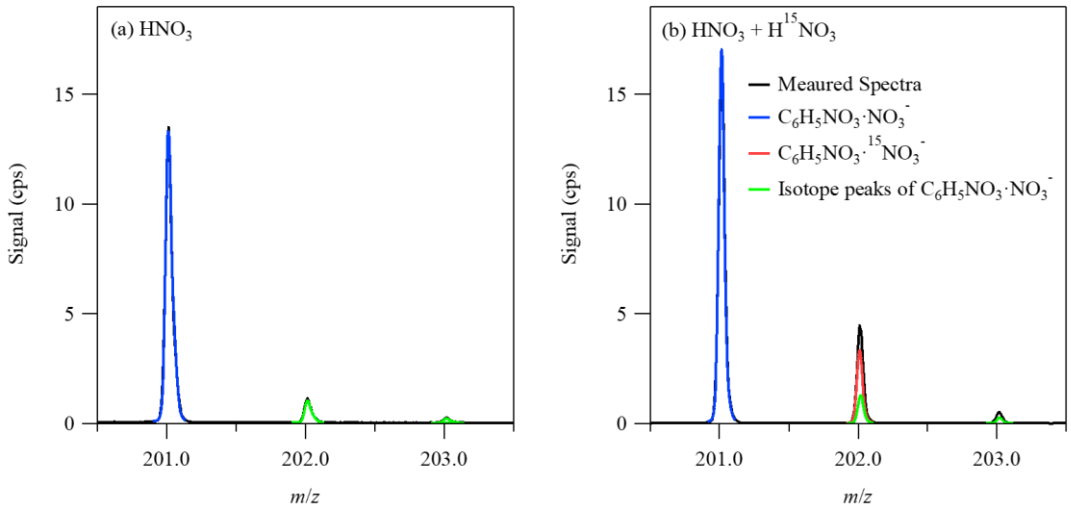

Figure S3. Average mass spectra of ambient air detected by the NO_3^--ToF-CIMS when using (a) nitric acid or (b) nitric acid and isotopically labelled nitric acid to produce the reagent ions. The colored peaks are the fitted ions of the spectra. The *m/z* range of 200.5 to 203.5 is shown as an example for $C_6H_5NO_3 \cdot NO_3^-$. Other NP$\cdot NO_3^-$ ions have similar features.

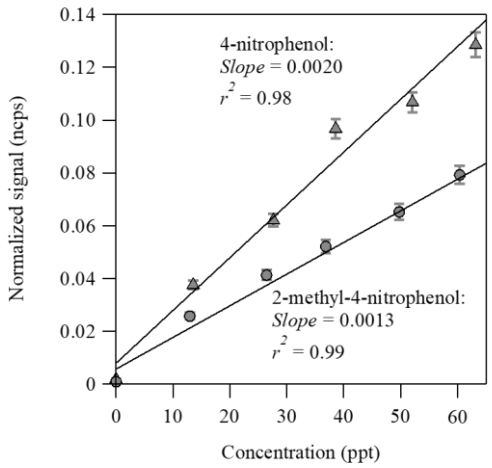

Figure S4. Calibration curves of 4-nitrophenol and 2-methyl-4-nitrophenol obtained from the permeation-tube method, all based on their NO_3^--adduct ions (Table 1). The slopes represent the sensitivities in unit of ncps ppt^{-1}.

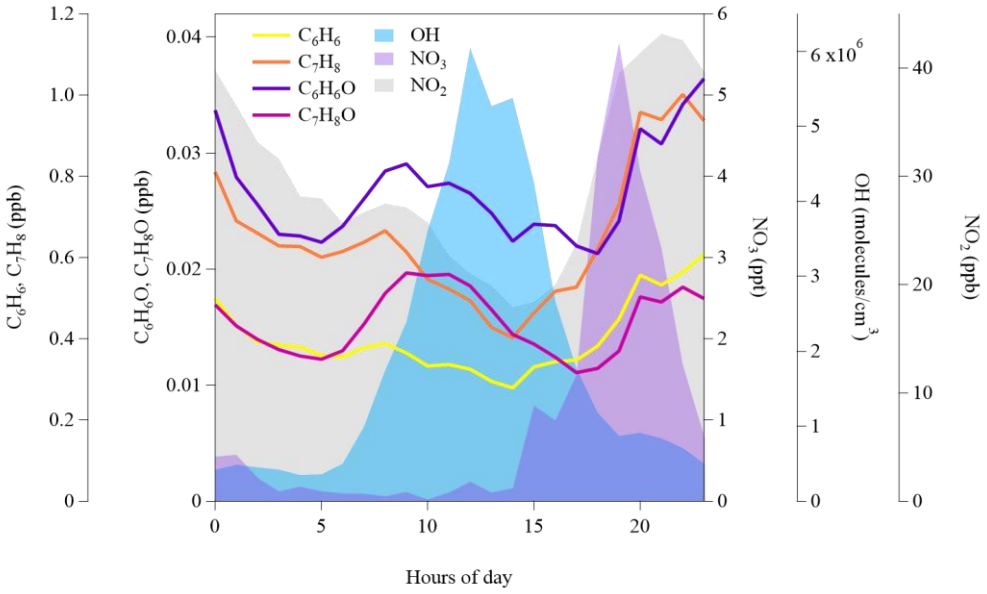

Figure S5. Diurnal profiles of the mean concentrations of OH and NO_3, NO_2, and key aromatic precursors of NPs. Phenol (C_6H_6O), cresol (C_7H_8O), benzene (C_6H_6), and toluene (C_7H_8) are measured by the PTR-QiToF.

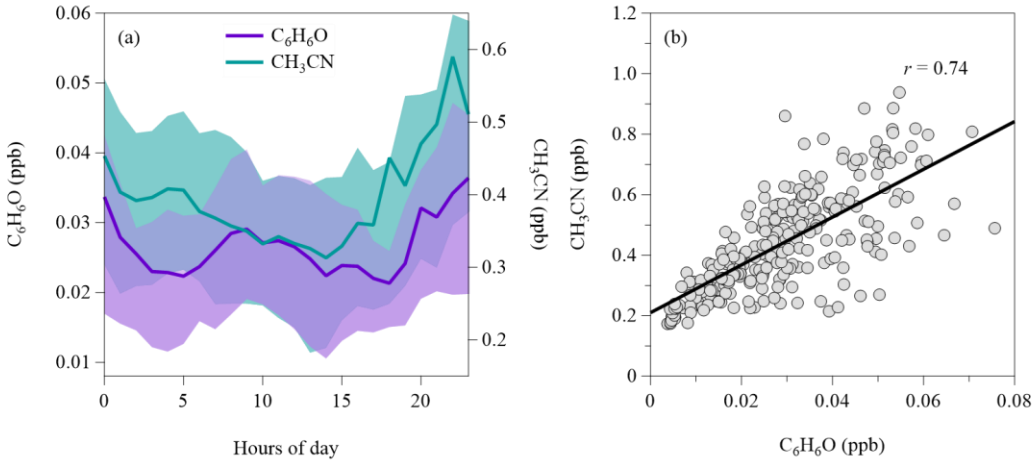

Figure S6. (a) Diurnal profiles of the mean concentrations of C_6H_6O and CH_3CN measured by the PTR-QiToF, the shaded areas represent the 25th and 75th percentiles. (b) Correlation of the nighttime concentrations of C_6H_6O and CH_3CN.

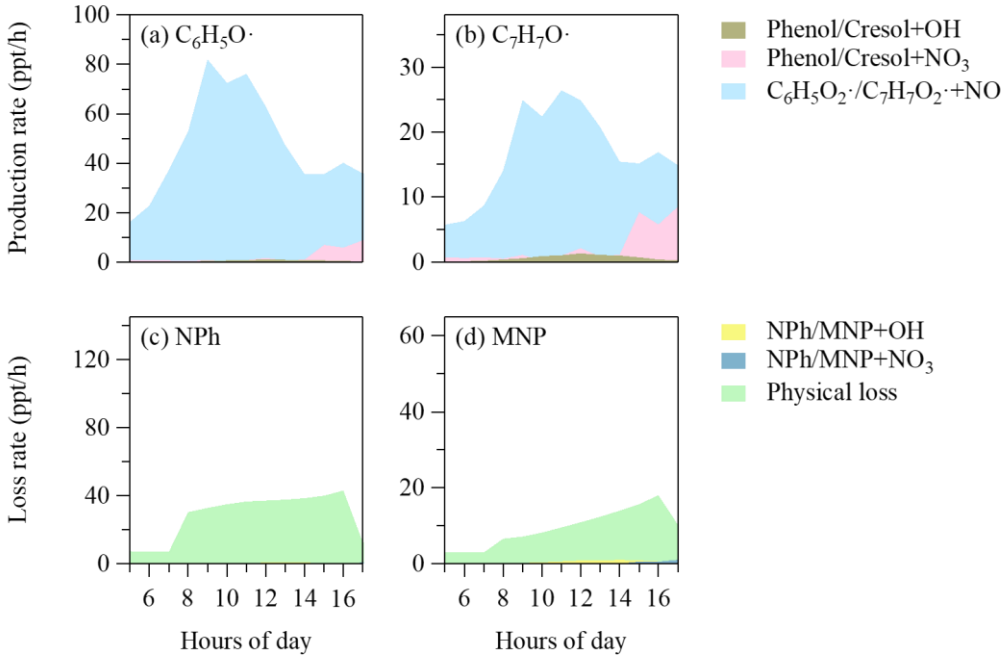

Figure S7. Mean diurnal profiles of (a, b) the chemical production rates of $C_6H_5O\cdot$ and $C_7H_7O\cdot$ from different pathways and (c, d) the chemical and physical loss rates for NPh and MNP.

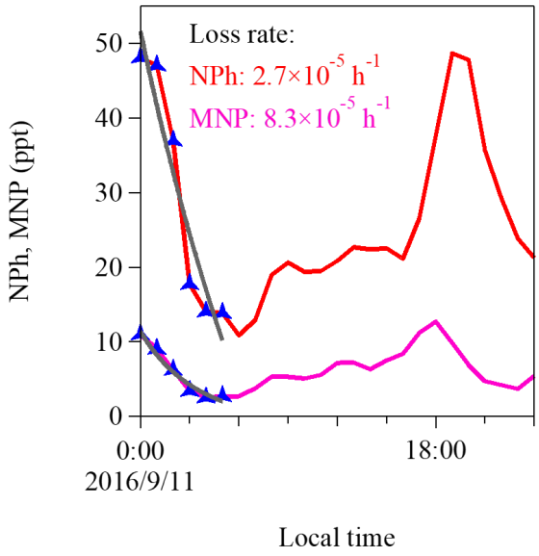

Figure S8. Example of the determination of nighttime physical loss rates by exponentially fitting to the concentrations of NPh and MNP between 12 a.m. and 5 a.m.

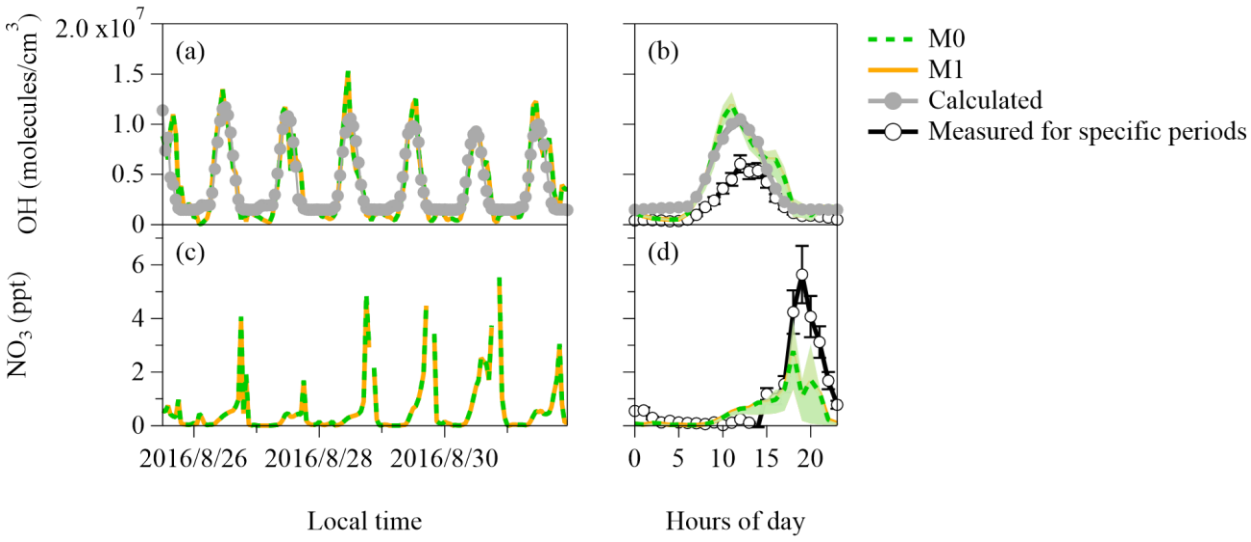

Figure S9. Time series and diurnal profiles of modeled and calculated (or measured) concentrations of: (a), (b) OH; (c), (d) NO_3 radicals. Calculated OH radicals were estimated using the empirical OH-J_{O^1D} relations. The measured OH and NO_3 concentrations corresponds to specific periods, i.e., OH measurement periods: 31 August-12 September 2016, 23 September-4 October 2016; NO_3 measurement periods: 11 September-4 October 2016. The uncertainties of measurements of ambient OH and NO_3 are ±14% and ±19%, respectively. Shaded areas represent the 25th and 75th percentiles.

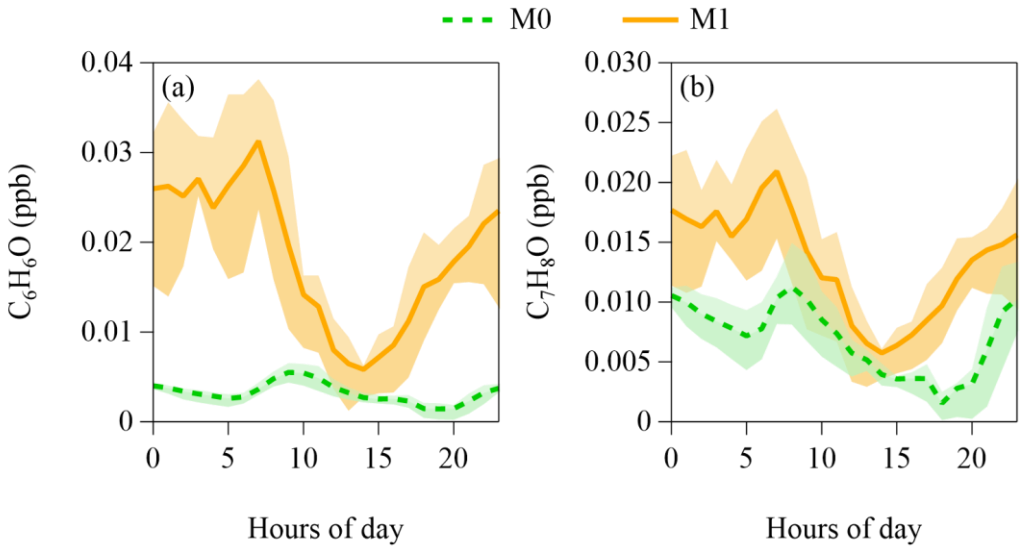

Figure S10. Diurnal profiles of the modeled and measured concentrations of (a) phenol (C_6H_6O) and (b) cresol (C_7H_8O) during the modeled periods. Measured concentrations of phenol and cresol are input to the model run of M1.

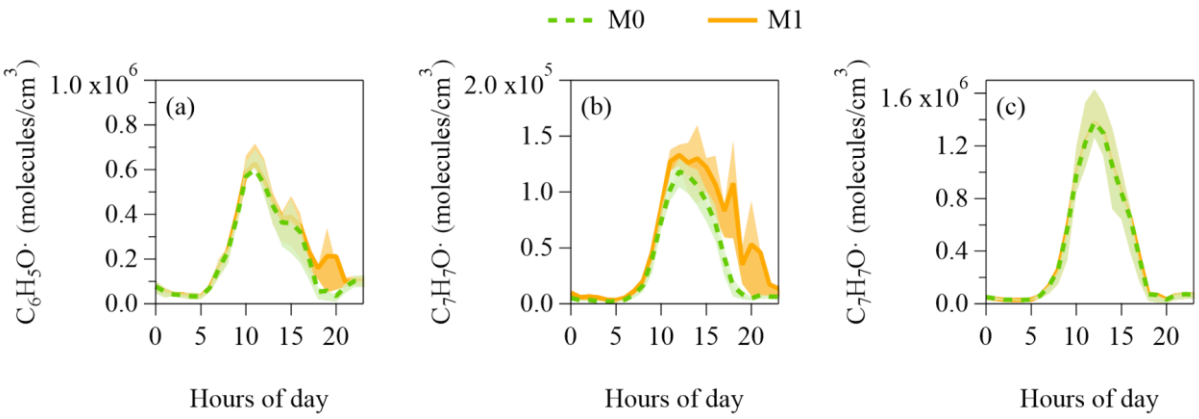

Figure S11. Diurnal profiles of modeled RO· concentrations. (a) C_6H_5O· (b) C_7H_7O· isomer (called as TOL1O in MCM), and (c) C_7H_7O· isomer (called as PXYL1O in MCM). Shaded areas represent the 25th and 75th percentiles.